Università degli Studi di Padova

Dipartimento di Ingegneria Industriale

Tesi di Laurea Magistrale in Ingegneria Aerospaziale

Anno accademico 2014-2015

Effect of particle density in a turbulent channel flow of dense suspensions

Relatore: *Dr.Ing. F. Picano*
Correlatore: *Prof. L. Brandt*
Correlatore: *Ing. W. Fornari*

Laureando: *Alberto Formenti*
Matricola: *1050127*

ma tu...balla, leggera
su questo prato di carta
mia Venere scalza
per te l'inchiostro è in offerta

Abstract

Several industrial applications deal with wall-bounded multi-phase flows, typical examples are oil pipelines and pharmaceutical industrial processes. These industrial flows are generally composed by an homogeneous mixture of a dispersed solid phase in a Newtonian fluid, called suspension, and are usually characterized by high velocities. Large part of previous studies considered the rheological properties of such flows in the laminar/viscous regime, whereas there is still a lack of knowledge of their behavior in the turbulent/inertial regime. Various parameters affect the properties of the flows of suspensions, e.g. the volume and the mass fractions of the suspended phase, or the shape and the density of the dispersed particles. This project aims to study the impact of the solid to fluid density ratio in a turbulent flow of suspensions. This effect is still unclear since both seminal and more recent investigations on turbulent suspensions mainly focus on the unitary density ratio. A suspension of rigid spheres in a Newtonian fluid at relatively high volume fractions is here studied in a plane channel geometry. Different values of the solid to fluid density ratio are considered in the range between 1 and 1000. The multi-phase flow is integrated through an Immersed Boundary Method to perform accurate Direct Numerical Simulations. The results show two different flow regimes occurring at relatively low and high density ratios and peculiar transport properties driven by the particle inertia.

Contents

Introduction

Suspensions of solid particles in liquid or gaseus flows are largely encountered in industrial applications and environmental flows. Typical examples of flows of suspensions are sediment transports, slurries, avalanches, gas and oil transports. These fluids normally flow at very high velocity. In these conditions, even restricting to a single-phase fluid, the inertia becomes important and gives rise to a chaotic regime with eddies and vortices called turbulence. More than a century of investigations testifies the difficulty in studying this regime. When a second phase is added, the analysis of this flow regime becomes even more complex. The present work aims both to recap the state of the art regarding the behavior of a flowing suspension and to investigate the response of the system to changes in the suspended phase properties and in particular in the solid to fluid density ratio.

Suspensions are generally constituted by a Newtonian liquid laden with solid particles that may differ for size, shape, density and stiffness. Their rheological properties were widely studied in the Stokesian regime, where the inertial effects are small compared to the viscous effects and can be safely neglected. Since simple analytical approaches are available for this regime, the behavior of suspensions in motion at negligible inertia is well understood (see Guazzelli and Morris, 2011 for a complete review on the topic). On the other hand, experimental and computational difficulties in the turbulent regime analysis have delayed the study of the flows of suspensions when their inertia becomes important. Previous studies focused on the behavior of these systems when the dispersed phase has a very low volume fraction ϕ. In this very dilute regime the particles slightly affect the suspension and they have a small effect on the flow. When the volume fraction increases, the behavior of the suspension dramatically changes. Lashgari et al. (see Lashgari et al., 2014) recently showed that the laminar-turbulent transition of a particle-laden flow is different from the single-phase problem: a third regime, called "inertial shear-thickening" appears in very dense suspensions. A first attempt to characterize the behavior of dense suspensions in the iner-

tial regime can be traced back to Bagnold (see Bagnold, 1954), who deduced the non-dimensional parameter Ba describing the transition from the viscous to the inertial regimes as a function of many suspension parameters, such as the volume fraction, the particle diameters, the dimensions of the domain and the density ratio. Recent numerical studies investigated the bulk properties of turbulent flows of suspensions when some of these parameters change. e.g. the volume fraction (see Picano et al., 2015). Nevertheless, the effects of a change of the suspended particle density are still not well characterized. The results reported in this work show that the changes in the particle density can produce similar effects to those found in previous studies where the volume fraction was much higher, e.g. an inertial shear-induced migration may occur. Different regimes are observed changing the density ratio R: the former typical of relatively light particles ($R \leq 10$), the latter of denser particles ($R \geq 100$). Moreover, the Bagnold number was found to be unable to describe the viscous-inertial transition when the density ratio is changed keeping fixed the other conditions.

The thesis is divided in four chapters. In the former the single-phase flows are introduced. The laws governing a simple flow in motion are shown and a brief introduction to turbulence and to channel flows is provided. The second chapter focuses on multi-phase flows and on all the problems related to the add of a second phase in the carrier fluid. In this chapter a review of the recent and more classical results about the flows of suspensions is outlined. The third chapter presents the methodology used in this project. In particular, the Computational Fluid Dynamics is briefly presented and then the main features of the Immersed Boundary Method are provided giving some specific details about the code used for the simulations carried out in this work. The last chapter shows the results obtained and discusses the consequence of the present findings in relation with the research background.

Chapter 1

Single-Phase Flows

In this first chapter the single-phase flows are introduced. After a brief introduction, the main equations describing a fluid flow are shown and the need of a mathematical approach for their resolution is explained. In the next sections a particular flow configuration called turbulence is examined and the theory depicting its behavior is provided. The last part of the chapter focuses on a particular class of bounded flows, the channel flows, representing the key subject of the following chapters of this work.

1.1 Fluids

Fluid is the state of matter which includes liquids, gases and plasmas:

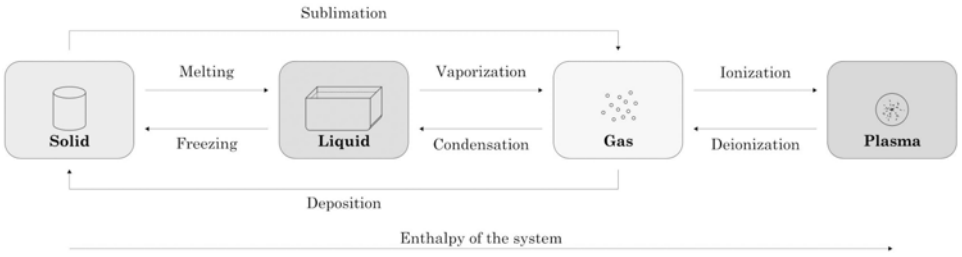

Figure 1.1: States of matter and transitions between different phases (Wikipedia).

Although it seems unambiguous, the distinction between solids and fluids is sometimes not obvious. It is common use to call solid a material which owns a preferred shape, and a fluid a material which takes the shape of its container. Mechanically, a fluid is defined as a substance that continually deforms under an applied shear stress, however small. The latter

specification is fundamental: in fact, even a solid material deforms continually if the applied shear stress exceeds a limiting value, corresponding to its "yield point". Anyway, below this value, solids tend to go back to their preferred shape, if the stress is no longer applied: they have a "perfect memory". Fluids instead never return to a preferred shape, after the stress is pulled back: they have "zero memory". This different behavior is not always pronounced: there are some materials presenting an intermediate behavior, with a "partial memory". In other words, they present both solid and fluid characteristics. Even tough solids and fluids behave very differently when subjected to shear stresses, they behave similarly under the application of compressive normal stress. Nevertheless, whereas a solid can support both tensile and compressive normal stresses, a fluid usually supports only compressive stresses. Fluids may be divided in three classes: liquids, gases and plasmas. A gas always expands and occupies the entire volume of any container. On the contrary, the volume of a liquid does not change much, so that it cannot always fill a large container. Plasmas are ionized gases, and mechanically they behave similarly to normal gases.

A fluid can be studied in rest (fluid statics) or in motion (fluid kinematics and fluid dynamics). Fluid statics, or hydrostatic, is fundamental to hydraulics, geophysics and medicine. On the other hand, fluid kinematics and fluid dynamics are applied in many engineering fields, such as mechanical and aerospace, and are fundamental for other disciplines such as meteorology and astrophysics. Fluid kinematics is the branch of mechanics which studies fluids and quantities involving space and time only. It treats variables such as displacements, velocities, accelerations, deformations and rotations of fluid elements without referring to the forces responsible for these motions. On the other hand, fluid mechanics is the branch of mechanics which studies the fluids and deals with the forces acting on them.

The laws governing fluid mechanics, and especially fluid dynamics, are complicated to treat and some of them still have no analytical solutions. For this reason, in many cases it is necessary to exploit numerical methods to compute their solution. A relatively new discipline, called Computational Fluid Dynamics (CFD), is dedicated to the numerical resolution of the problems involving the fluid motion. Although the mathematical basics of this discipline are quite old, the CFD has shown its potentially only in the second part of the last century, with the increase of computer power.

1.2 Fluid Dynamics

Fluid dynamics is the branch of fluid mechanics focused on the study of fluid flows. Let us consider a spatial domain $\mathcal{D} \in \mathbb{R}^3$ and a temporal interval $[0, T] \in \mathbb{R}$. Fluid dynamics is based on three conservation laws:

-conservation of mass:

$$\frac{\partial \rho}{\partial t} + \nabla \cdot (\rho \boldsymbol{u}) = 0 \tag{1.1}$$

-conservation of linear momentum:

$$\rho \frac{\partial \boldsymbol{u}}{\partial t} + \rho \boldsymbol{u} \cdot \nabla \boldsymbol{u} = \nabla \cdot \boldsymbol{\sigma} + \rho \boldsymbol{f} \tag{1.2}$$

-conservation of energy:

$$\rho \frac{\partial h}{\partial t} + \rho \boldsymbol{u} \cdot \nabla h = \rho \frac{\partial p}{\partial t} + \rho \boldsymbol{u} \cdot \nabla p + \nabla \cdot (k \nabla T) + \phi \tag{1.3}$$

where, in the above equations, the field $\rho(\boldsymbol{x}, t)$ is the density of the fluid, the field $\boldsymbol{u}(\boldsymbol{x}, t)$ is its velocity, $\boldsymbol{\sigma}$ is the tensor of the stresses, h is the enthalpy, p is the pressure, k is the thermal conductivity, T is the temperature and ϕ is the viscous dissipation function. Note that, if the flow is steady, meaning that its properties do not change over time, all time-dependent terms in the above equations disappear.

For a fluid in motion, the tensor $\boldsymbol{\sigma}$ is given by:

$$\boldsymbol{\sigma} = -p\boldsymbol{I} + \boldsymbol{\tau} \tag{1.4}$$

where I is the identity tensor and $\boldsymbol{\tau}$ is the tensor of viscous stresses. Substituting Eq. (1.4) in Eq. (1.2), it is easy to obtain the following expression of the conservation of the linear momentum:

$$\rho \frac{\partial \boldsymbol{u}}{\partial t} + \rho \boldsymbol{u} \cdot \nabla \boldsymbol{u} = -\nabla p + \nabla \cdot \boldsymbol{\tau} + \rho \boldsymbol{f} \tag{1.5}$$

In Eq. (1.5), the terms of right hand-side represents the pressure force, the viscous forces and the mass forces acting on the fluid, respectively. For most of the usual fluids, such as air or water, the tensor of viscous stresses is given by the well-know Newtonian law:

$$\boldsymbol{\tau} = \lambda \boldsymbol{I} \nabla \cdot \boldsymbol{u} + 2\mu \boldsymbol{D} \tag{1.6}$$

where μ is the dynamic viscosity and $\boldsymbol{D}$ is the tensor of strain rate:

$$\boldsymbol{D_{i,j}} = \frac{1}{2}\left(\frac{\partial u_i}{\partial x_j} + \frac{\partial u_j}{\partial x_i}\right) \tag{1.7}$$

If the fluid has a tensor of viscous stresses linearly dependent to the tensor of strain rate, i.e. given by Eq. (1.6), it is called Newtonian fluid, otherwise it is said to be non-Newtonian. If the tensor of viscous stresses $\boldsymbol{\tau}$ is instead null, the flow is said to be non-viscous.

The flows studied in this work are incompressible: a flow is compressible if a change in pressure or temperature results in a change of the density; if this does not happen, or if the change of the density is negligible, the flow is incompressible. For an incompressible flow it easy to obtain from Eq. (1.1) the following expression:

$$\nabla \cdot \boldsymbol{u} = 0 \tag{1.8}$$

If the fluid is Newtonian and the flow is incompressible, its motion is governed by the well-know Navier-Stokes equations:

$$\frac{\partial \boldsymbol{u}}{\partial t} + \boldsymbol{u} \cdot \nabla \boldsymbol{u} = -\frac{1}{\rho}\nabla p + \nu \nabla^2 \boldsymbol{u} + \boldsymbol{f} \tag{1.9a}$$

$$\nabla \cdot \boldsymbol{u} = 0 \tag{1.9b}$$

In Eq. (1.9a) each term has a proper physical meaning:

-the first term on the left hand side represents the temporal evolution of an instantaneous field of velocity;

-the second term on the left hand side is the convection of the velocity field, which is nonlinear and responsible for fluctuations;

-the first term on the right hand side describes the effect of the gradient of the pressure on the fluid;

-the second term on the right hand side represents the effect of viscous forces, i.e. the momentum diffusion and the dissipation of kinetic energy into thermal energy;

-the last on the right hand side is the mass force term.

The system of Equations (1.9a)-(1.9b) needs specific initial and boundary conditions to be solved. The initial conditions, which should be necessarily a solenoidal field, can be generally expressed in the domain $\mathcal{D}$ as:

$$\boldsymbol{u}(\boldsymbol{x}, t) = \boldsymbol{u_0}(\boldsymbol{x}) \quad \text{per} \quad \boldsymbol{x} \in \mathcal{D} \tag{1.10}$$

For the boundary conditions, both velocity or strain can be assigned. It is in fact possible to divide the border of the domain in a part where the quantity assigned is the velocity and another where it is the strain:

$$\boldsymbol{u}(\boldsymbol{x},t) = \boldsymbol{u}_{\partial}(\boldsymbol{x},t) \quad \text{per} \quad \boldsymbol{x} \in \partial\mathcal{D}_V, \tag{1.11a}$$

$$\boldsymbol{t}(\boldsymbol{x},t) = \boldsymbol{t}_{\partial}(\boldsymbol{x},t) \quad \text{per} \quad \boldsymbol{x} \in \partial\mathcal{D}_T \tag{1.11b}$$

The system of Equations (1.9a)-(1.9b), together with the boundary conditions (1.11a)-(1.11b), and initial conditions (1.10), is said to be a *well posed problem* if:

-the solution exists;

-the solution is unique;

-the solution depends continuously on the data.

For the Navier-Stokes equations, none of these three points has been mathematically demonstrated so far, although the experimental datas suggest that the first two points are generally verified. The third condition is strictly related to the sensitivity to the initial data. Let us consider two generic initial states $\boldsymbol{u}_o(\boldsymbol{x})$ and $\boldsymbol{u}'_o(\boldsymbol{x})$, which differ for a small value less than an assigned arbitrarily small δ_ε, and their respective solutions $\boldsymbol{u} = \boldsymbol{u}(\boldsymbol{x},t)$ and $\boldsymbol{u'} = \boldsymbol{u'}(\boldsymbol{x},t)$; if the maximum of the difference between these last solutions is smaller than ε, then the third point is verified.

$$\begin{aligned} &\text{if} \parallel \boldsymbol{u}_o(\boldsymbol{x}) - \boldsymbol{u}'_o(\boldsymbol{x}) \parallel \;\leq\; \delta_\varepsilon \\ \Rightarrow \quad &\max_t \parallel \boldsymbol{u}(\boldsymbol{x},t) - \boldsymbol{u'}(\boldsymbol{x},t) \parallel \;\leq\; \varepsilon \quad \forall t \geq 0. \end{aligned} \tag{1.12}$$

This is the typical behavior of the so-called "laminar flows": two "near" initial conditions evolve into two "near" solutions. On the other hand, in a so-called "turbulent flow" this condition takes place only for $t \leq T_\varepsilon$, where T_ε is a typical time called separation time, dependent on δ_ε: smaller δ_ε are associated to longer time length, beyond which it is not possible to define ε anymore. Therefore laminar flows are said to be stable; for turbulent flows instead, after the time T_ε (which decreases with the non-dimensional parameter Re, called the Reynolds number), the solutions are instantly totally different: they are unstable. The phenomenon that is observed at a generic instant $t > T_\varepsilon$ is called developed turbulence phenomenology; this fact introduces the existence of stochastic solutions, although the Navier-Stokes equations are purely deterministic.

The unsimplified Navier-Stokes are then impossible to solve analytically. To this date, their complete resolution is possible only with mathematical methods, and this represents the main reason of using computers to perform calculations. However, sometimes even for computers the direct resolution of Navier-Stokes problem is too demanding. In these cases, some simplifications can be made upon the equations: these simplifications lead to an easier and faster resolution of the Navier-Stokes equations and some of them, under appropriate conditions, allow to solve the fluid flow in a closed form.

1.3 Dynamic Similarity

Dynamic Similarity is the discipline consecrated to the study of problems through non-dimensional parameters. For fluid dynamics in particular the idea is to relate two flows having different length-scales, flow speed or fluid properties, if the values of these non-dimensional parameters are comparable. The principle of dynamic similarity is at the heart of experimental fluid mechanics, in which the datas should be unified and presented in non-dimensional terms. The concept of similarity is also indispensable for designing models in which tests can be conducted for predicting the flow properties of full-scale objects.

Non-dimensional parameters can be deduced directly from the governing differential equations, when known. From the Navier-Stokes equations it is easy to obtain a crucial non-dimensional parameter for Fluid Dynamics, the Reynolds number:

$$Re = \frac{ul}{\nu} \tag{1.13}$$

In Eq. (1.13) u represents the velocity, l the characteristic length and $\nu = \frac{\mu}{\rho}$ the kinematic viscosity. The Reynolds number represents the ratio between inertial and viscous forces: if it is much lower than the unity, the inertial forces can be neglected in comparison with the viscous forces; on the contrary, if the Reynolds number is high, the viscous forces are negligible if compared to the inertial forces and the approximation of non-viscous flow can be assumed.

Through the Navier-Stokes equations it is possible to deduce another important non-dimensional parameter, representing the weight of the local acceleration compared to the viscous term of Equations (1.9a)-(1.9b):

$$St = \frac{l^2}{T\nu} \tag{1.14}$$

where T is the characteristic time-scale. This parameter is called the Stokes number.

If $Re \ll 1$ and $St \ll 1$, the system of Equations (1.9a)-(1.9b) can be reduced to the so-called Stokes Equations:

$$-\frac{1}{\rho}\nabla p + \nu\nabla^2\boldsymbol{u} + \boldsymbol{f} = 0 \tag{1.15a}$$

$$\nabla\cdot\boldsymbol{u} = 0 \tag{1.15b}$$

If $Re \ll 1$ but the Stokes number is not negligible, it is necessary to keep from Eq. (1.9a) the unsteady term $\rho\frac{\partial \boldsymbol{u}}{\partial t}$. In this case, the resulting equations are called the unsteady Stokes Equations.

1.4 Turbulence

A key subject of this thesis work is the turbulence. The are many possibilities to observe turbulent flows in everyday experiences: the smoke arising from a burning cigarette, the water skimming aside a boat in rapid motion, the buffeting of a strong wind are only a few examples of turbulent flows. In engineering applications, turbulent flows are prevalent: flows of liquids or gases in pumps, compressors, pipe lines, flows surrounding airplanes, automobiles and ships are generally turbulent.

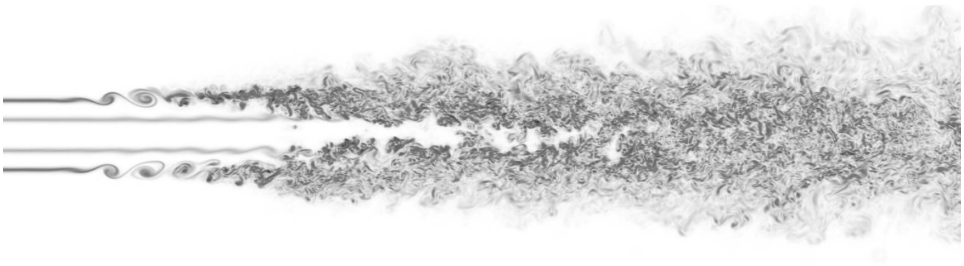

Figure 1.2: Example of a transition to turbulence in a subsonic co-axial jet flow (Prof. Dr. L.Kleiser).

1.4.1 Reynolds Equations

A turbulent flow is characterized by an irregular fluid velocity change over both time and space. In each direction i, the velocity field $u_i(x_i, t)$ can be decomposed in a mean term $U_i(x_i, t)$ and in a fluctuations term $u_i'(x_i, t)$, which can be over a quarter of the mean velocity value:

$$u_i(x_i, t) = U_i(x_i, t) + u_i'(x_i, t) \tag{1.16}$$

The mean term is defined by the ensemble average:

$$U_i = \langle u_i(x, t) \rangle = \lim_{N \to \infty} \frac{1}{N} \sum_{n=1}^{N} u_i^n(x, t) \tag{1.17}$$

where N is the number of used realizations. A direct consequence of this definition is the zero value of the ensemble average of the fluctuating term:

$$\left\langle u_i'(x_i, t) \right\rangle = 0 \tag{1.18}$$

It is anyway important to underline that the ensemble average of the square of the fluctuation is generally not null:

$$\left\langle u_i'^2(x_i,t)\right\rangle \neq 0 \tag{1.19}$$

In fact, the root square of this quantity can be used as a significant reference value of the fluctuations:

$$u_{rms} = \sqrt{\left\langle u_i'^2\right\rangle} \tag{1.20}$$

This decomposition, called the Reynolds decomposition, can be applied in the same way to every physical quantity, for example to the pressure p , to the stress tensor $\boldsymbol{\sigma}$ and to forces $\boldsymbol{f}$.

With the Reynolds decomposition, the Navier-Stokes equations (1.9a)-(1.9b) are transformed in the Reynolds equations:

$$\frac{\partial U_i}{\partial t} + U_j\frac{\partial U_i}{\partial x_j} = -\frac{1}{\rho}\frac{\partial p}{\partial x_i} + \nu\frac{\partial^2 U_i}{\partial x_j \partial x_j} - \frac{\partial\left\langle u_i' u_j'\right\rangle}{\partial x_j} + f_i \tag{1.21a}$$

$$\frac{\partial U_i}{\partial x_i} = 0 \tag{1.21b}$$

The only difference with Eq. (1.9a)-(1.9b) is the term $\frac{\partial\langle u_i' u_j'\rangle}{\partial x_j}$. In order to understand its meaning, let us rewrite Eq. (1.21a) as follow:

$$\rho\left(\frac{\partial U_i}{\partial t} + U_j\frac{\partial U_i}{\partial x_j}\right) = \frac{\partial}{\partial x_i}\left[\mu\left(\frac{\partial U_i}{\partial x_j} + \frac{\partial U_j}{\partial x_i}\right) - p\delta_{i,j} - \rho\left\langle u_i' u_j'\right\rangle\right] \tag{1.22}$$

The first term of the right hand side represents the viscous stress, arising from momentum transfer at the molecular level. The second term is the isotropic stress, appearing from the mean pressure field. The last term is the so-called Reynolds stress term and represents the stress given by the fluctuating velocity field. More precisely, it arises from the mean momentum flux due the fluctuating velocity. This value represents the key problem of turbulent flow: if it is not zero, the system is nevermore set in a closed-form. The four equations of the Reynolds problem (the three components of the Reynolds equations and the continuity equation) have more than four unknowns: in addition to the velocity (three components) and the pressure, there are also the Reynolds stresses. In this form, the Reynolds equations cannot be solved unless the Reynolds stresses are somehow determined.

1.4.2 The Scales of Turbulence

Turbulent flows are rotational. A flow is rotational if the vorticity is not equal to zero. The vorticity is the quantity that describes the local spinning motion of a fluid near some point, in other words its tendency to rotate. Many phenomena, such as the blowing out of a candle by an air gust, are more readily explained in terms of vorticity rather than the basic concepts of pressure and velocity.

The vorticity $\boldsymbol{\omega}(\boldsymbol{x}, t)$ is found to be equal to the curl of the velocity:

$$\boldsymbol{\omega} = \boldsymbol{\nabla} \times \boldsymbol{u} \tag{1.23}$$

The curl of the momentum equation results in the following equation:

$$\frac{\partial \omega}{\partial t} + (u_i \cdot \nabla)\,\omega = (\omega \cdot \nabla) u_j - \omega \nabla \cdot u_j + \frac{1}{\rho^2}(\nabla\rho \times \nabla\rho) + \nu \nabla^2 \omega \tag{1.24}$$

Eq. (1.24) is the vorticity transport equation. In this equation, the four terms on the right hand side represent physical different mechanism affecting the transport of the vorticity: the first of these terms describes the mechanism of the energy cascade, the second term represents the impact of compression and expansion on vorticity, the third terms is responsible for generating a torque due to dissimilar acceleration of light and high density fluid, and the last term describes the viscous diffusion of vorticity.

Because of their rotational nature, turbulent flows are characterized by the presence of eddies of many different length-scales. An eddy is loosely defined as coherent patterns of velocity, vorticity and pressure. The extent of an eddy is described with a characteristic length, l. Eddies of size l have a characteristic velocity $u(l)$ and timescale $\tau(l) = l/u(l)$. Largest eddies are characterized by a length-scale l_0 comparable to the flow scale L, and their velocity $u(l_0)$ is on the order of the r.m.s. turbulence intensity, $u' = \frac{2}{3}k^{\frac{1}{2}}$, where $k = 2\pi/l$ is the wavelength.

Large eddies are unstable and normally break up, and transfer their energy to smaller eddies. As represented in Fig. (1.3), the energy continues to pass on to smaller eddies until a very small spatial scale at which the molecular viscosity is effectively dissipating the kinetic energy into heat.

The whole process was summarized by Richardson in 1922:

Big whorls have little whorls,
Which feed on their velocity;
And little whorls have lesser whorls.
And so on to viscosity
(in the molecular sense).

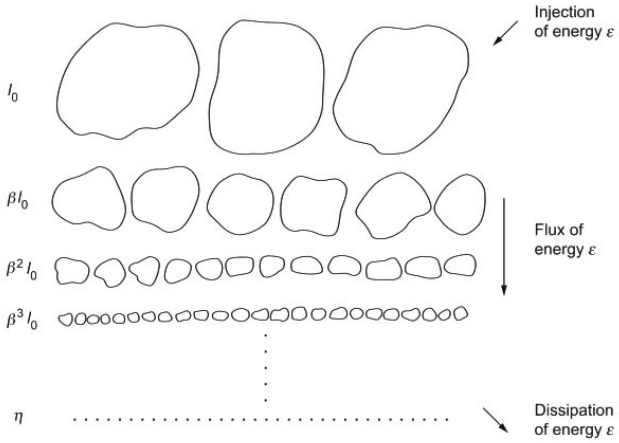

Figure 1.3: Representation of the energy cascade (Frisch).

At large flow scales, the rate of energy dissipation ϵ is governed by the energy transfer from the large eddies, in other words the whole process is governed by the first process in sequence. Furthermore, the kinetic energy of the eddy scales quadratically with the characteristic eddy velocity u_0^2. The energy cascade is then found to scale with $\frac{u_0^2}{\tau_0}$.

A big contribute to the study of scales of turbulent motion was given by the studies of Kolmogorov. His theory (see Kolmogorov 1941a,b) is stated in the form of two hypotheses:

-the first hypotheses states that the small scale flow motion is statically isotropic in high Reynolds number and uniquely governed by the kinematics viscosity ν and the dissipation rate ϵ. Note that the isotropy entails that the directional biases of the large scales are completely lost in the chaotic scale-reduction process, by which the energy is transferred to smaller eddies. The length-scale where the transition anisotropic-istropic eddies is found to appear is l_{EI} (around $1/6l_0$). As a consequence to this first hypotheses, given the two parameters ϵ and ν, there are only one length, one velocity and one time-scale that can be formed for the small scale flow. These are the Kolmogorov scales:

$$\eta = \left(\nu^3/\epsilon\right)^{1/4} \tag{1.25a}$$

$$u_\eta = (\epsilon/\nu)^{1/4} \tag{1.25b}$$

$$\tau_\eta = (\nu/\epsilon)^{1/2} \tag{1.25c}$$

-the second hypotheses states that in every turbulent flow at sufficient high Reynolds number, the statistics of the motion of scale l in the range

$\eta \ll l \ll l_0$ have a universal form that is uniquely determined by ϵ, independent of ν. From Eq. (1.25a)-(1.25c) it is possible to obtain the scaling from large to small eddies based on the Reynolds number:

$$\eta/l_0 \sim Re^{(-3/4)} \tag{1.26a}$$

$$u_\eta/u_0 \sim Re^{(-1/4)} \tag{1.26b}$$

$$\tau_\eta/\tau_0 \sim Re^{(-1/2)} \tag{1.26c}$$

At sufficiently high Reynolds number, there is a range of scales l that are very small compared to l_0 but very large compared to η. In this case, the high Reynolds number makes their motion only slightly affected by the viscosity. Hence, the unique key parameter for such eddies is ϵ.

Let us now introduce the length-scale l_{DI}. From the above hypotheses, it is then possible to to divide the equilibrium range (for high Reynolds number flows) in two parts:

-the dissipation range: the motion experiences significant viscous effects;

-the inertial subrange: the motion is determined only by inertia.

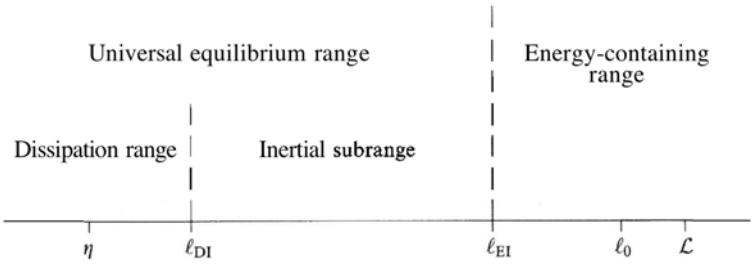

Figure 1.4: Eddy size l (on a logarithmic scale) at very high Reynolds number, showing the various length-scales and ranges (Pope).

Summarizing, through the energy cascade, a turbulent flow can be realized as a superposition of a spectrum of velocity fluctuations and eddies upon a mean flow. It may be viewed as made of an entire hierarchy of eddies over a wide range of length-scales and the hierarchy can be described by the energy spectrum that measures the energy in velocity fluctuations for each length-scale (wavenumber). Dimensional analysis implies that the energy spectrum E of homogeneous turbulence in the equilibrium range can be expressed as:

$$E(k) \sim g\left(\nu^{3/4}\epsilon^{-1/4}k\right)\epsilon^{2/3}k^{-5/3} \tag{1.27}$$

where, as already stated, k is the wavelength of length-scale l flow.

1.5 Channel Flows

Most of turbulent flows appearing in engineering applications are bounded (at least in part) by one or more solid surface. Examples are internal flows such as the flow through pipes and ducts, external flows such as the flow around aircraft and ships' hulls and flows in the environment such as the atmospheric boundary layer. Key parameters of these problems are the form of velocity profiles and the friction laws, describing the shear stress exerted by the fluid on the wall. This paragraph focuses on the channel flow. Since this study concerns only this kind of flow, other important examples of internal bounded flows, such as pipe flows, are not treated.

Let us consider a flow through a rectangular duct, which has height h=2δ , large length ($L \gg \delta$) and aspect ratio ($b \gg \delta$). The mean flow is predominantly in the spanwise ($x = x_1$) direction, with the mean velocity varying mainly in the wall-normal ($y = x_2$) direction. The bottom and top walls are at $y = 0$ and $y = 2\delta$, respectively, with the mid-plane being $y = \delta$. The extent of the channel in the spanwise ($z = x_3$) direction is large compared with δ so that (remote from the end walls) the flow is statistically independent of z. The centerline is defined by $y = \delta$, $z = 0$. The velocities in the three coordinate directions are $(u, v, w) = (u_1, u_2, u_3)$, with mean values $(U, V, W) = (U_1, U_2, U_3)$ and fluctuations $(u', v', w') = (u_1, u_2, u_3)$. The mean spanwise velocity w is zero.

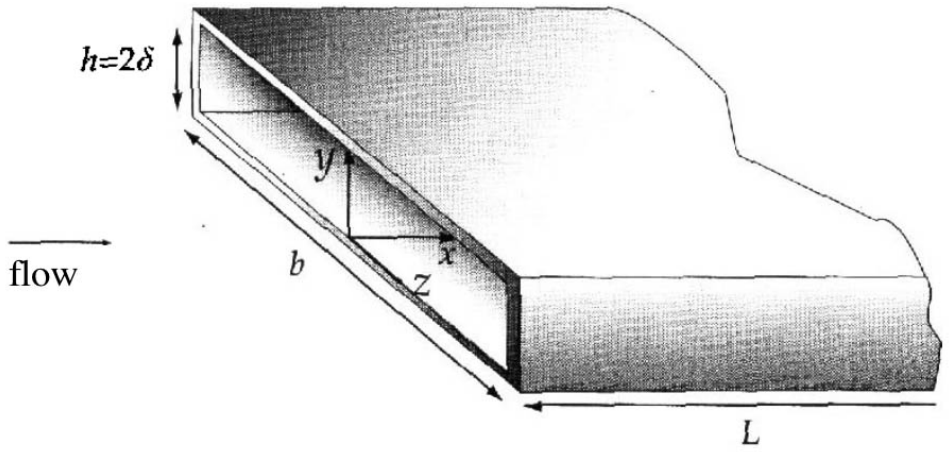

Figure 1.5: Sketch of a channel flow (Pope).

The attention focuses on fully developed region, far from $x = 0$. The flow is treated as statically stationary and statically one-dimensional, with velocity statistics depending only on y.

The Reynolds numbers used to describe the flow are:

$$Re_b = u_b 2\delta/\nu \tag{1.28}$$

$$Re_0 = u_0 \delta/\nu \tag{1.29}$$

where u_0 is the centerline velocity and u_b is the bulk velocity:

$$u_b = \frac{1}{\delta}\int_0^\delta U\, dy \tag{1.30}$$

The flow is laminar for $Re_b < 1350$ and fully turbulent for $Re_b > 3000$.

1.5.1 Forces in Channel Flows

The mean continuity equation (1.21b), reduces to:

$$\frac{dv}{dy} = 0 \tag{1.31}$$

since $w = 0$ and u is not dependent of x. The boundary condition $v_{y=0}$ leads to say that v is zero for all y.

The mean-momentum equations (1.21a) reduce to:

-Lateral:

$$0 = -\frac{1}{\rho}\frac{\partial p}{\partial y} - \frac{\partial \left\langle v'^2 \right\rangle}{dy} \tag{1.32}$$

-Axial:

$$0 = -\frac{1}{\rho}\frac{\partial p}{\partial y} + \nu\frac{d^2u}{dy^2} - \frac{\partial \left\langle u'v' \right\rangle}{dy} \tag{1.33}$$

The combination of these equations leads to an important result:

$$\frac{d\tau}{dy} = \frac{dp_w}{dx} \tag{1.34}$$

where the total shear stress is:

$$\tau = \rho\nu\frac{dU}{dy} - \rho\left\langle u'v' \right\rangle \tag{1.35}$$

Since τ is a function only of y and p_w is a function only of x, it follows from Eq. (1.34) that both solutions have to be constants. The solution for both $\tau(y)$ and dp_w/dx can be written in terms of the wall shear stress $\tau_w = \tau(0)$, leading to:

$$\frac{dp_w}{dx} = -\frac{\tau_w}{\delta} \tag{1.36}$$

$$\tau(y) = \tau_w \left(1 - \frac{y}{\delta}\right) \tag{1.37}$$

To summarize: the flow is driven by a drop in pressure between the entrance and the exit of the channel. In the fully developed region there is a constant (negative) mean pressure gradient, which is balanced by the shear stress gradient. For a given pressure gradient dp_w/dx and channel half-width δ, the linear shear stress profile is independent of the fluid properties (e.g., ρ and ν), and independent of the state of fluid motion (i.e., laminar or turbulent). If the flow is defined by p, v, δ, and dp_w/dx, then u_0 and u_b are not known a priori.

From Eq. (1.35), the shear stress is found to be equal to the sum of the viscous stresses and the Reynolds stresses. However, at the wall the velocity is zero, so the Reynolds stresses disappears. In proximity of the wall is then useful to define some parameters representing the velocity scales and length-scales of this region:

-the friction velocity:

$$u_\tau = \sqrt{\frac{\tau_w}{\rho}} \tag{1.38}$$

-the viscous length:

$$\delta_\nu = \nu\sqrt{\frac{\rho}{\tau_w}} = \frac{\nu}{u_\tau} \tag{1.39}$$

-the friction Reynolds number:

$$Re_\tau = \frac{u_\tau \delta}{\nu} = \frac{\delta}{\delta_\nu} \tag{1.40}$$

-the distance from the wall measured in viscous lengths:

$$y^+ = \frac{y}{\delta_\nu} = \frac{u_\tau y}{\delta_\nu} \tag{1.41}$$

-the mean fluid velocity measured in inner units:

$$u^+ = \frac{u}{u_\tau} \tag{1.42}$$

1.5.2 Velocities in Channel Flows

Using some of the new parameters above described, it is possible to find different regions of the flow:

-inner layer: there is a direct effect of molecular viscosity on the shear stress;

-outer layer: the direct effect of molecular viscosity on the shear stress is negligible.

Within these regions it is also possible to define:

-viscous sublayer (inner layer): the Reynolds shear stresses are negligible compared to the viscous stresses;

-buffer layer (inner layer);

-log law region (inner layer);

-overlap region (outer layer).

Each of these regions is defined by a particular mean velocity profile. In order to study the profile of the velocity, it is more appropriate to look at the quantity dU/dy. There are many reasons to do so, one of them is that the viscous stress and the turbulence production are both determined by that quantity. dU/dy is found to depend on just two parameters, so it is possible to write:

$$\frac{dU}{dy} = \frac{u_\tau}{y}\Phi\left(\frac{y}{\delta_\nu}, \frac{y}{\delta}\right) \tag{1.43}$$

where Φ is a universal non-dimensional function. These two parameters are chosen because δ_ν is the appropriate length-scale in the inner layer, and δ is the appropriate scale in the outer layer.

Near the wall, the mean fluid velocity in inner units results:

$$U^+ = y^+ + \mathbb{O}\left(y^{+2}\right) \tag{1.44}$$

The departures from the linear relation $U^+ = y^+$ are negligible in the viscous sublayer, but are significant (greater than 25%) starting from the buffer layer region.

Getting away from the wall, in the so-called log-law region, the viscosity has no longer direct effects on the velocity. The new expression of the mean fluid velocity is:

$$U^+ = \frac{1}{k}\ln y^+ + B \tag{1.45}$$

where k is the so-called von Karman constant and B an additive coefficient. Typical values of these two constants are:

$$k = 0.41 \quad \text{and} \quad B = 5.2 \tag{1.46}$$

The region between the viscous sub-layer and the log-law region is called the buffer layer. This region is characterized by the transition from the viscosity-dominated and the turbulence-dominated parts of the flow.

Unlike the inner part of the channel, for higher values of y^+ (outer layer) there are no universal expressions describing the evolution of the mean fluid velocity: each flow is governed by its own law.

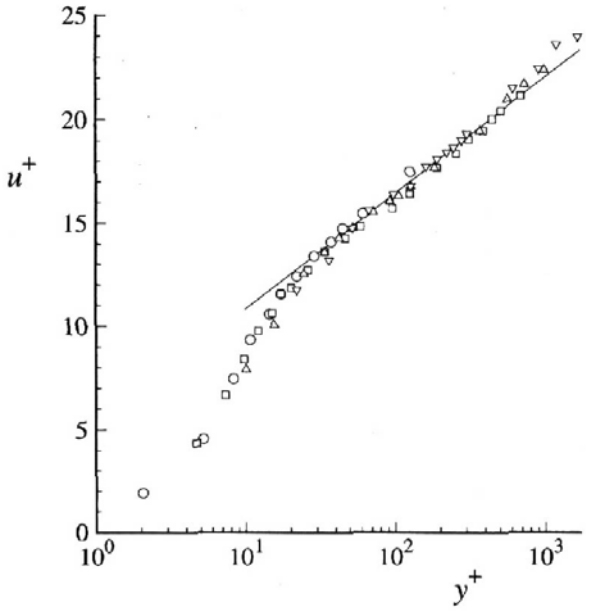

Figure 1.6: Mean velocity profile in fully developed turbulent channel flow: $\circ$:$Re_0 = 2970$, $\square$:$Re_0 = 14914$, $\triangle$:$Re_0 = 22276$, ∇:$Re_0 = 39582$, Line: Log-Law Eq. (1.45) (Pope).

Chapter 2

Multi-Phase Flows

In this second chapter the multi-phase flows and the flows of suspensions are treated. Firstly, the general equations governing the different phases in a multi-phase flow are presented. In the second part the interactions between different phases and between two different parts of the discontinue phase are examined. In the following section some hypothesis, and in particular the approximation of finite inertia, are overcame and the consequences of this change is shown. The last section focuses on multi-phase channel flows, both in laminar and turbulent regime, with particular attention given to recently published results. Large part of the present chapter was extracted by the Guazzelli and Morris book "A Physical Introduction to Suspension Dynamics" to which the reader can refer for more details.

2.1 General Equations

In fluid mechanics, a multi-phase flow is a flow where two or more phases are present. The most common situation is a two-phases flow. The latter occurs for example in a system containing solid particles immersed in a continuous fluid, with a meniscus separating the two phases. In this case, if the mixture is heterogeneous and the solid particles are sufficiently large for sedimentation, the system is called suspension. In a multi-phase flow each of the phases is considered to have separately defined volume fractions (the sum of which is equal to one) and velocity fields.

Let us consider a bi-phase flow composed by spherical solid spheres dispersed in a general continuous fluid. The motion of the fluid is governed by the Navier-Stokes equations. The influence of the presence of a different phase arises from the boundary conditions which they impose upon the fluid motion. The first set of boundary conditions (at infinity or at wall)

remains unchanged, but a new set of boundary conditions at the interface particles-fluid is needed. The usual condition is that there is no slip at the surface of the particle, meaning that the velocity of the fluid at a point in contact with a particle surface is the same as the particle velocity at this point. This condition can be written at the surface of the particle as:

$$\boldsymbol{u}(\boldsymbol{x}) = \boldsymbol{u}^P + \boldsymbol{\omega}^P \times (\boldsymbol{x} - \boldsymbol{x}_{com}) \tag{2.1}$$

where $\boldsymbol{x}_{com}$ is the coordinate of the center of mass, $\boldsymbol{u}^P$ is the translational velocity and $\boldsymbol{\omega}^P$ is the rotational velocity of the particle. This condition must be indicated for each particle, and since the particles are usually in motion, the problem is time-dependent.

In many practical flows of suspensions the Reynolds number (1.13) and the Stokes number (1.14) are small: for a grain of sand of size $l = 1\mu m$, for example, the settling velocity in water is about $u = 1\mu m/s$ and the characteristic sedimenting time is $T \ll 10^{-6}s$. It is then admissible to reduce the Navier-Stokes equations (1.9a)-(1.9b) to the simpler Stokes equations (1.15a)-(1.15b). The advantage of using the Stokes approximations is the lost of the nonlinear convective acceleration and of the time-dependent terms in the Navier-Stokes equations. The suppression of the nonlinear term makes the new equations linear, so that a change in the magnitude of the forcing is linearly reflected in the fluid velocity: a doubling of the driving pressure gradient in a pressure-driven Stokes channel flow, for example, yields a doubling of the flow rate. Moreover, the linearity allows the use of the principle of the superposition: the motion of the suspended particle can be decomposed in a translation plus a rotation around its center of mass.

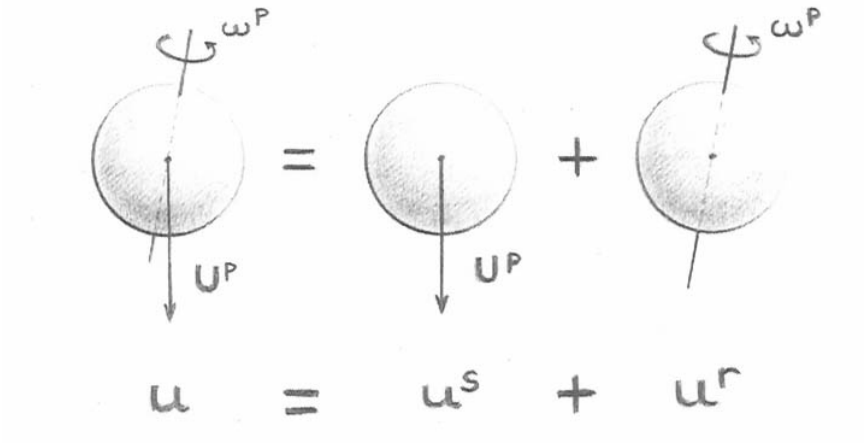

Figure 2.1: Summation of rotation and translation (Guazzelli).

The linearity implies also that the motion is reversible in the driving force, so that if the driving force is reversed, the particle velocity must be reversed too. On the other hand, the suppression of the time-dependency implies that the predicted motion is quasi-static, and that there is no history dependence of the fluid motion. The boundary conditions, both inner (fluid-solid interface) and outer (fluid and environment), are instantly communicated to the entire fluid. Obviously, this is just a mathematical simplification and the physical reality is slightly different, since it is well-known that every information needs a finite time to propagate within a medium.

2.2 Stokes flows

2.2.1 One sphere in Stokes flow

In order to understand how a bi-phase flow globally behaves, it is necessary to first understand how the two phases, fluid and solid in this case, interact. Let us firstly consider the simplest situation: a single spherical particle immersed in a Stokes flow. The fluid motion near a point $\boldsymbol{x_0}$ can be described by a Taylor series:

$$\boldsymbol{u}^{\infty}(\boldsymbol{x}) = \boldsymbol{u}^{\infty}(\boldsymbol{x_0}) + \nabla \boldsymbol{u}^{\infty}(\boldsymbol{x_0}) \cdot (\boldsymbol{x} - \boldsymbol{x_0}) + ... \tag{2.2}$$

where $\boldsymbol{u}^{\infty}$ is the velocity field in absence of any disturbance due to the presence of the particle. Neglecting the higher order terms in the series, assuming $\boldsymbol{x} - \boldsymbol{x}_0$ small, the velocity results a sum of an uniform translation plus a linearly varying field. Taking $\boldsymbol{x}_0$ as the origin and $\boldsymbol{u}^{\infty}(\boldsymbol{x}_0) = \boldsymbol{u}^{\infty}$, the expression of the velocity can be therefore expressed as:

$$\boldsymbol{u}^{\infty}(\boldsymbol{x}) = \boldsymbol{u}^{\infty} + \boldsymbol{\Omega}^{\infty} \cdot \boldsymbol{x} + \boldsymbol{E}^{\infty} \cdot \boldsymbol{x} \tag{2.3}$$

where the two tensors are defined as follow:

$$\Omega_{i,j}^{\infty} = \frac{1}{2}\left[\frac{\partial u_i^{\infty}}{\partial x_j} - \frac{\partial u_j^{\infty}}{\partial x_i}\right] \quad E_{i,j}^{\infty} = \frac{1}{2}\left[\frac{\partial u_i^{\infty}}{\partial x_j} + \frac{\partial u_j^{\infty}}{\partial x_i}\right] \tag{2.4}$$

The first tensor is the rate of rotation tensor while the second is the rate of strain tensor. The particle is then subjected at the same time to a translation, to a rotation and to a strain.

The presence and the motion of a particle within a fluid flow generate a disturbance field for both velocities and pressures, from those existing in the imposed flow in absence of the body:

$$\boldsymbol{u}(\boldsymbol{x}) = \boldsymbol{u}^{act}(\boldsymbol{x}) - \boldsymbol{u}^{\infty}(\boldsymbol{x}) \tag{2.5}$$

$$p(x) = p^{act}(x) - p^{\infty}(\boldsymbol{x}) \tag{2.6}$$

where $\boldsymbol{u^{act}}$ and p^{act} are the the actual fluid motion and the actual pressure field, respectively.

Let us consider separately the disturbance fields caused by translation, rotation and straining. The problem to solve is given by the homogeneous Stokes equations for the disturbance fields:

$$\mu\nabla^2\boldsymbol{u} = \nabla p \tag{2.7a}$$

$$\nabla\cdot\boldsymbol{u} = 0 \tag{2.7b}$$

These three situations have different boundary conditions:
-for translation:

$$\boldsymbol{u} = -\boldsymbol{u}^{\infty} \quad \text{at} \quad r = |\boldsymbol{x}| = a \tag{2.8a}$$

$$\boldsymbol{u}, p \to 0 \quad \text{as} \quad r = |\boldsymbol{x}| \to \infty \tag{2.8b}$$

-for rotation:

$$\boldsymbol{u} = -\boldsymbol{\omega}^{\infty} \times \boldsymbol{x} \quad \text{at} \quad r = |\boldsymbol{x}| = a \tag{2.9a}$$

$$\boldsymbol{u}, p \to 0 \quad \text{as} \quad r = |\boldsymbol{x}| \to \infty \tag{2.9b}$$

-for straining:

$$\boldsymbol{u} = -\boldsymbol{E}^{\infty}\cdot\boldsymbol{x} \quad \text{at} \quad r = |\boldsymbol{x}| = a \tag{2.10a}$$

$$\boldsymbol{u}, p \to 0 \quad \text{as} \quad r = |\boldsymbol{x}| \to \infty \tag{2.10b}$$

where a is the radius of the particle.

The disturbance velocity and the disturbance pressure for a general coordinate (i, j, k) are given by:
-for translation:

$$p(x_i) = -\frac{3\mu a}{2}\frac{U_j^{\infty}x_j}{r^3} \tag{2.11a}$$

$$u_i = \frac{3a}{4}u_j^{\infty}\left(\frac{\delta_{ij}}{r} + \frac{x_i x_j}{r^3}\right) - \frac{3a^3}{4}u_j^{\infty}\left(\frac{\delta_{ij}}{3r^3} + \frac{x_i x_j}{r^5}\right) \tag{2.11b}$$

The disturbance fields decay very slowly away from the translating sphere, as r^{-2} for the pressure, as r^{-1} for the dominant portion of the velocity and as r^{-3} for the other portion of the velocity;

-for rotation:

$$p\left(x_i\right) = 0 \tag{2.12a}$$

$$u_i = -\varepsilon_{ijk}\omega_j^{\infty} x_k \left(\frac{a}{r}\right)^3 \tag{2.12b}$$

The disturbance field for velocity decays as r^{-2}, while there is no pressure induced by the presence of a rotating particle in a static fluid (or symmetrically by the presence of a fixed particle in a rotating fluid);

-for straining:

$$p\left(x_i\right) = -5\mu a^3 \frac{x_i E_{ij}^{\infty} x_j}{r^5} \tag{2.13a}$$

$$u_i = -\frac{5a^3}{2}\frac{x_i x_j E_{jk}^{\infty} x_k}{r^5} - \frac{a^5}{2} E_{jk}^{\infty}\left[\frac{\delta_{ij}x_k + \delta_{ik}x_j}{r^5} - \frac{5x_i x_j x_k}{r^7}\right] \tag{2.13b}$$

The disturbance field for pressure decays as r^{-3}, while the disturbance field of the velocity has a portion decaying as r^{-2} and another one decaying more rapidly as r^{-4}.

The fluid stress field acting from the fluid on the particle results in a:

-hydrodynamic force:

$$\boldsymbol{F}^h = \int_{Sp} \boldsymbol{\sigma}\cdot\boldsymbol{n}\, dS \tag{2.14}$$

-hydrodynamic torque:

$$\boldsymbol{T}^h = \int_{Sp} \boldsymbol{x}\times\boldsymbol{\sigma}\cdot\boldsymbol{n}\, dS \tag{2.15}$$

-hydrodynamic stresslet: this term, less known than the previous, form the complete first moment together with the torque:

$$M_{ij} = \int_{Sp} \sigma_{ik} n_k x_j\, dS = S_{ij} + A_{ij} \tag{2.16}$$

where S is the symmetric portion (called stresslet):

$$S_{ij} = \frac{1}{2}\int_{Sp} \left[\sigma_{ik}x_j + \sigma_{jk}x_i\right] n_k\, dS \tag{2.17}$$

and A is the anti-symmetric portion, related to the value of the torque:

$$A_{ij} = \frac{1}{2}\int_{Sp} \left[\sigma_{ik}x_j - \sigma_{jk}x_i\right] n_k\, dS \tag{2.18}$$

In particular, for a spherical particle immersed in a general flow field these three quantities result:

-hydrodynamic force:

$$\boldsymbol{F} = 6\pi\mu a \left[\left(1 + \frac{a^2}{6}\nabla^2 \right) \boldsymbol{u}^{\infty} \left(\boldsymbol{x} = 0 \right) - \boldsymbol{u}^{P} \right] \tag{2.19}$$

This value scales linearly with the size of the sphere;

-hydrodynamic torque:

$$\boldsymbol{T} = 8\pi\mu a^3 \left[\boldsymbol{\omega}^{\infty} \left(\boldsymbol{x} = 0 \right) - \boldsymbol{\omega}^{P} \right] \tag{2.20}$$

This value scales linearly with the cube of the size of the sphere;

-hydrodynamic stresslet:

$$\boldsymbol{S} = \frac{20}{3}\pi\mu a^3 \left(1 + \frac{a^2}{10}\nabla^2 \right) \boldsymbol{E} \left(\boldsymbol{x} = 0 \right) \tag{2.21}$$

This value scales linearly with the cube of the size of the sphere.

If a single particle, and in particular a freely mobile particle (meaning that it has no external influence upon the fluid and experiences no hydrodynamic forces and torques) is immersed in a simple shear flow, i.e. a flow of the form $\boldsymbol{u}^{\infty} = (\dot{\gamma}, 0, 0)$, the situation is different. In this case, the velocity at the surface of the particle is found to be equal to the sum of the ambient shear flow and the disturbance flow generated by the particle. The latter is due only to its resistance to the straining component of the shearing flow.

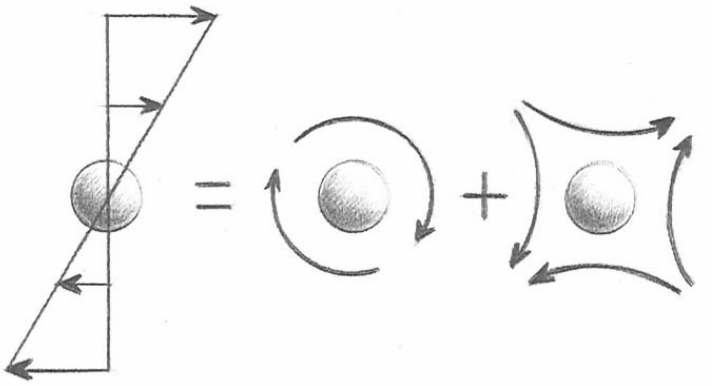

Figure 2.2: Decomposition of a sphere in a shear flow by a sphere in a rotation plus a sphere in strain (Guazzelli).

2.2.2 Two spheres in Stokes flow

If there is more than one particle, not only the fluid-particle interaction has to be considered. An hydrodynamic interaction between the particles arises: the fluid motion induced by one particle affects the motion of the other particles and vice-versa. More in detail, the velocity field created by one particle considered in isolation induces a velocity disturbance at the center of the other particle which causes this latter to move; this movement have in turn influence on the first particle and so on.

If there are two particles, this interaction can be described as follow:

$$\begin{Bmatrix} \boldsymbol{u}_1 \\ \boldsymbol{u}_2 \end{Bmatrix} = \begin{bmatrix} \boldsymbol{M}_{11} & \boldsymbol{M}_{12} \\ \boldsymbol{M}_{21} & \boldsymbol{M}_{22} \end{bmatrix} \cdot \begin{Bmatrix} \boldsymbol{F}_1^e \\ \boldsymbol{F}_2^e \end{Bmatrix} \tag{2.22}$$

where the above tensors depend on the flow analyzed and on the properties of the particles. The off-diagonal tensors $\boldsymbol{M}_{12}$ and $\boldsymbol{M}_{21}$ are the new quantities introduced by the hydrodynamic interaction above mentioned.

The interaction between the particles becomes more and more relevant as they approach. When their surfaces get closer, they experience a phenomenon called lubrication:

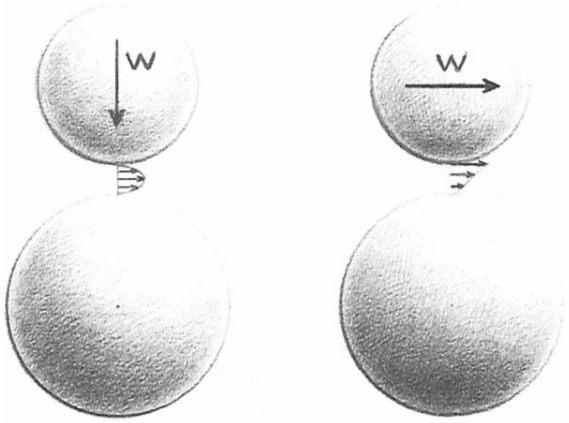

Figure 2.3: Squeezing and shearing problem (Guazzelli).

Lubrication is here described in two particular situations: in the squeeze flow problem two spheres with the same radius a move along their line of centers with relative velocity $\boldsymbol{w}_{sq}$. In the shear flow problem instead, the two spheres move on the same direction, so the relative velocity $\boldsymbol{w}_{sh}$ is perpendicular to the line of centers. The distance between the two surface is ϵ and in both cases is very small. In either case, the force necessary to impose the motion at the same speed $\boldsymbol{w}$ diverges as ϵ approaches to zero:

$$F_{sq} \sim \mu a w \epsilon^{-1} \qquad \text{in squeeze flow problem} \tag{2.23a}$$

$$F_{sh} \sim \mu a w \ln \epsilon \qquad \text{in shear flow problem} \tag{2.23b}$$

Physically, as the gap decreases the pressure becomes very large on a small area surrounding the two spheres. Even though this area is very small, it is not small enough to avoid the divergence of the imposed force. In the same way, since the motion is reversible, as the gap between the particles increases, an equally large negative pressure is imposed and the resulting force has the same magnitude but opposite sign.

2.2.3 Suspensions in Stokes flow

When the number of particles suspended in the main continuous fluid starts to become remarkable, the overall viscosity of the new flow increases as the volume fraction of the particles becomes large. This increase is due to the opposition made by every single particle to the flow strain. In other words, the stress on the non-deforming particle surface results in a disturbance flow, which enhance the dissipation energy. The growth of the viscosity value is given by the following equation:

$$\mu_S = \mu \left[1 + \frac{5\phi}{2} \right] \tag{2.24}$$

This is the so-called Einstein viscosity. This expression was found to fit the real viscosity only for low volume fraction, i.e. below 5%. For higher values of the volume fraction, the experimental results diverge from this prediction and a more accurate expression is necessary. A second-order model for predicting the suspension viscosity as a function of the volume fraction was proposed by Batchelor and Green (see Bachelor and Green, 1972):

$$\mu_S = \mu \left[1 + \frac{5\phi}{2} + 6.95\phi^2 \right] \tag{2.25}$$

For a multi-phase flow, the value of the volume fraction cannot increase up to the unity. There is in fact a limit, under a simple shear flow, above which the viscosity is so high that the fluid can nevermore flows. This value was found to be equal to about 0.55.

When the number of suspended particles increases, other important phenomena arises. In particular, if a shear flow is imposed, two unexpected and irreversible behaviors appear: shear-induced diffusion and shear-induced migration. These effects were found to be due to the combined effects of non-hydrodynamic and hydrodynamic interactions among suspended particles.

Shear-induced diffusion is characterized by significant fluctuations of particles paths from their average motion: this means that there are generally lateral (y and z) components of any particle velocity. For purely hydrodynamically interacting suspensions of spheres, this shear-induced diffusion is unexpected: the diffusion should in fact be reversible, based on the linearity.

Shear-induced migration is a phenomenon firstly described by Leighton and Acrivos (see Leighton and Acrivos, 1987): the particles tend to migrate irreversibly from the high shear rate region towards the low shear rate region. This migration was observed even for suspensions of non-Brownian spheres carefully designed to be neutrally buoyant in the suspending fluid.

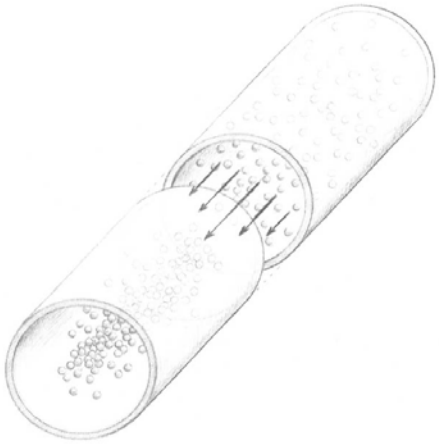

Figure 2.4: Shear induced migration
in a pressure-driven flow (Guazzelli).

Moreover, various applications (see Koh et al., 1994 and Nott and Brady, 1994) showed this migration even at small Reynolds number. This observation is crucial since it shows that inertia is not the leading parameter of the phenomenon. A simple equation was proposed by Leighton and Acrivos (see Leighton and Acrivos, 1987) to model the shear-induced migration flux:

$$\boldsymbol{j}_{\perp} \sim -a^2 \nabla \dot{\gamma} \tag{2.26}$$

where a indicates the value of the particle radius. This equation was found to match well with the experimental results for linear flows, but it is no longer valid for curvilinear flows.

2.3 Finite-inertia flows

The approximations of Stokes flows assumed up to this point is not always valid. In particular, in a real multi-phase flow it is necessary to take into account the influence of fluid and particle inertia on the overall process. The inclusion of the inertia changes the form of motion equations, even if the value of this inertia is small.

Let us consider the simple situation of a fixed spherical particle in an uniform flow $\boldsymbol{u}$. Far from the sphere, the velocity field for zero Reynolds number is given by $\boldsymbol{u} + \mathbb{O}(ua/r)$ and the disturbance is $\boldsymbol{u'} = \mathbb{O}(ua/r)$. The ratio between inertial and viscous effects is then given by:

$$\frac{|[(\boldsymbol{u}+\boldsymbol{u'})\cdot\nabla]\,(\boldsymbol{u}+\boldsymbol{u'})|}{|\nu\nabla^2\,(\boldsymbol{u}+\boldsymbol{u'})|} \sim \frac{ua}{\nu}\frac{r}{a} = Re\frac{r}{a} \tag{2.27}$$

From this equations it is easily deduced that when $r/a \ll Re^{-1}$ the inertial effects can be neglected. On the contrary, at positions far from the sphere they become comparable to the viscous effects. The approximation of Stokes flow is thus not valid for uniform flows past the sphere when $r/a \geq Re^{-1}$. This result was obtained and summarized by Oseen (see Oseen, 1910). He proposed, even for high Reynolds number flows, to consider the inertial forces only in the far field, where their value are comparable with them of the viscous forces, and to neglect them in the region of the flow near the particle, where the influence of the inertia on the process is minimal. The method of resolution for the resulting Navier-Stokes equations involves simultaneous consideration of locally valid expansions in the inner (near the particle) and in the outer (far from the particle) regions of the flow. The inner expansion is required to satisfied the no-slip condition on the particle, while the outer expansion needs to satisfy the uniform-flow condition at infinity. These expansions are then combined through a process called matching to obtain an approximate solution for the whole domain.

In pressure-driven flows, when finite-inertia is considered, another migrational phenomenon arise. However, contrary to shear-induce migration, which is driven by the particle-particle interaction, this inertial migration results from the fluid-particle interaction within the confining geometry of a conduit. In pressure-driven flows at small-finite inertia the particles tend to pinch to a preferred position. In tubes (or channels), for example, particles which initially are at a larger r (or h) are driven inward, whereas particles to the centerline are driven outward. There is an equilibrium position where the particles tend to align into extended and long-lived trains forming a sort of annulus (see Segré and Silberberg, 1962). This annulus becomes unstable

when the Reynolds number increases: in this case the particles tend to form another annulus but closer to the centerline.

If the considered flow is a simple-shear flow under finite-inertia, the situation is slightly different. Two different cases have to be considered: the first is the case of finite particle inertia ($St > 0$) and negligible fluid inertia ($Re = 0$), while the second case includes similar density for fluid and solid phases ($Re > 0$ and $Re \approx St$). In the first case, it was recently found by Subramanian and Brady (see Subramanian and Brady, 2006) that if a pair of dense particles is placed in such a flow, their trajectory deviate from the trajectory followed by a neutrally-buoyant pair when the trajectory is curved, resulting in an accelerating flow. The second case, when the fluid inertia is not neglected anymore, is more complicated, since the fluid flow is not governed anymore by the Stokes equations. The complete form of the Navier-Stokes equations has to be considered and this leads to important results: the lost of linearity causes the lost of symmetry of fluid streamlines, which results in a inflow of fluid along the vorticity axis, with spiraling motion in the other two directions.

2.4 Suspensions in channel flows

Let us focus again on a particular type of flow, the channel flow, already analyzed in Section (1.5) for single-phase flows. In real applications it is more common that a channel flow results formed by more than one phase mixed together: examples of such situations are pipelines for oil and pharmaceutical applications. The study of a multi-phase flow within a channel is much more complicated than the single-phase one: first of all, more parameters are involved in the analysis, and the effects of each one on the overall process are far from being completely understood. Secondly, it is common opinion that the influence of these parameters changes if the volume fraction ϕ of the suspended solid phase increases, but it is still not clear how and why these changes show up. Moreover, while many previous studies investigated the properties of dense particle suspensions in the laminar regime, little is known on the behavior of these suspensions in the turbulent regime.

This section is dedicated to recap the results on the behavior of suspension flows published up to this date. The first part concerns the definition of the regimes of a suspension flow, and in particular the laminar-turbulent transition problem. The second part focused on the differences between dilute and dense suspension behaviors: the specific background representing the starting point of this thesis is here showed, the main results obtained are presented and the reason of this work is eventually explained.

2.4.1 Laminar-turbulent transition

When a flow of suspensions is considered, the particle-particle interactions significantly alter the bulk behavior, in particular in the transition regime. Recent works such as Matas et al. (see Matas et al., 2003) and Yu et al. (see Yu et al., 2013) underlined the difficulties to distinguish unambiguously the flow regime of dense suspensions since they manifest important fluctuations even at low velocities. The recent publication of Lashgari et al. (see Lashgari et al., 2014) focused on this topic and characterized the flow regimes of suspensions of finite-size rigid particles in a viscous fluid at finite inertia.

Lashgari et al. identified three different flow regimes for a channel flow of suspensions, with a smooth transition between them:

-a "laminar like" regime (Blue zone in Fig.(2.5)), at low Re and low ϕ, dominated by viscous forces;

-a "turbulent like" regime (Red zone in Fig.(2.5)), at high Re and sufficiently low ϕ, where the wall friction due to the turbulent transport increases;

-an "inertial shear-thickening" regime (Green zone in Fig.(2.5)), at high Re and high ϕ, characterized by a significant increase of the wall friction (and then of the effective viscosity), larger than in the "turbulent like" regime: this enhancement is not related to the increase of the Reynolds stresses, but to an increase of the particle-induced stress, which indicates a transport mechanism different than that of the turbulence.

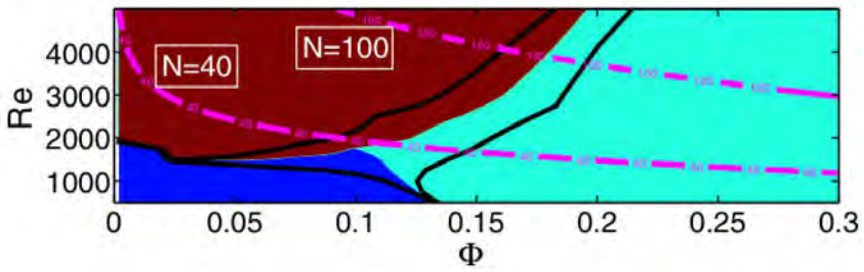

Figure 2.5: Phase diagram for a channel flow of suspensions.
The black lines represents the boundary of the regions where each term in the stress budget is over 50% of the total stress.
The purple lines are the isolevels of Bagnold number (Lashgari et al.).

Summarizing, at low volume fractions ϕ, the flow becomes turbulent when increasing the Reynolds number, transitioning from the laminar regime dominated by viscous forces to the turbulent regime characterized by enhanced momentum transport by turbulent eddies. At larger volume fractions ϕ, Lashgari et al. identified a new regime characterized by an even larger

increase of the wall friction. The wall friction increases with the Reynolds number (inertial effects) while the turbulent transport is weakly affected, as in a state of intense inertial shear-thickening: this state may prevent the transition to a fully turbulent regime at arbitrary high speed of the flow.

2.4.2 Dilute and dense suspensions in turbulent flows

If the volume fraction of the suspended phase is low, the suspension is said to be a dilute suspension, otherwise it is called a dense suspension. For dilute suspensions the most important interactions arising in a flow are the particle-fluid interactions, while for dense suspensions the hydrodynamics and collisional interactions among the particles become crucial.

The work entitled "Two-way coupled turbulence simulations of gas- particle flows using point-particle tracking" by Eaton (see Eaton J.K., 2009) well summarizes the numerical and experimental results achieved for dilute suspensions and demonstrates the effects of particle loadings on a multi-phase flow in turbulent regime. Many experiments (see Kulick et al., 1994, Paris and Eaton, 2001) carried out at Stanford University showed that carrier phase turbulence properties are highly influenced by the presence of dispersed particles even in very simple flows. In particular, suspensions with low volume fraction but high density ratio (then high mass fraction) were tested. Kulick et al. found that increasing the mass loading ration up to 80% the turbulence was essentially eliminated near the channel centerline. Moreover, Paris and Eaton found that the turbulence attenuation was dependent also on the particle Reynolds number. In particular, the biggest attenuations of the turbulence were found in those cases where the particle diameter was of the same order as the Kolmogorov scale. On the other hand, many issues arose in numerical simulations: first of all, the typical grid sizes in direct numerical simulation codes were found to be not fine enough to fully resolve the flow around an individual particle, and at the same time the particles were too large to reasonably be represented as a point; the second problem concerned the inter-particle spacing for dilute suspensions flows: if the grid had the resolution of the particle diameter, then most grid cells would not contain any particles. This issue is particularly crucial for bounded flows, where the presence of walls require a very high grid resolution. The fully resolved simulations reported in the work of Eaton checked the local turbulence modification around individual particles in a dispersed flow: the three dimensional and time-dependent fluid motion was calculated in an Eulerian frame, while a large number of particles were tracked in a Lagrangian frame. The main result was the demonstration that the local

affects of the particle were reducing the turbulence over a fluid volume of at least 1000 times the particle volume. However, for small volume fractions, this local reduction was not found to be spread in the global field.

When the volume fraction increases the situation changes. The recent work of Picano et al. (see Picano et al., 2015) investigated the turbulent channel flow at high volume fractions ϕ. The results obtained were very interesting: as shown in Fig. (2.6(a))-(2.6(b)), if the volume fraction (then the mass fraction) is increased with a unitary density ratio, the turbulence is attenuated in the same way described by Eaton. Moreover, they noticed that the increase of the number of particles in the channel leads to a redistribution of the energy towards a more isotropic state: in fact, while in the streamwise direction the fluctuations were found to decrease with ϕ, in the wall-normal and spanwise directions they increased. Only at very high values of ϕ the fluctuations were found to decrease with respect to all the other cases, with the exception of a thin region close to the wall. In this small region the fluctuations enhanced because of the squeezing motion occurring between the wall and an incoming or outgoing particle.

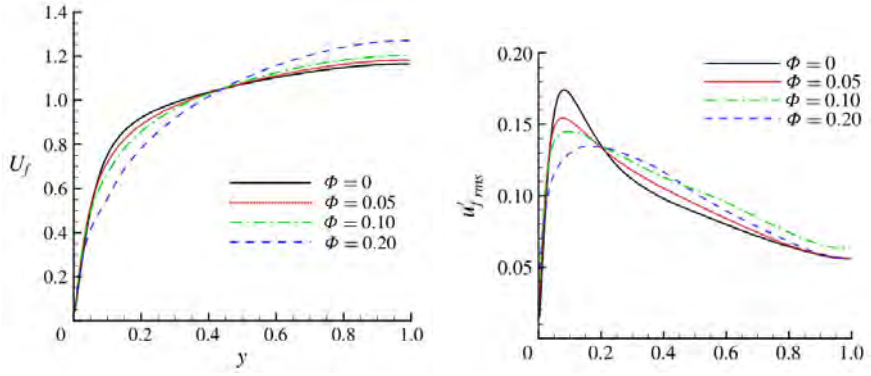

(a) (b)

Figure 2.6: a) Mean fluid velocity and b) fluctuation velocity components in the streamwise direction.

In many previous works the mean local particle distribution was studied. Fig. (2.7) shows a first local maximum around $y = 0.05 - 0.1 \simeq a(= 1/18)$, and a local minimum at $y = 0.1 - 0.15 \simeq 2a(= 1/9)$. As shown in Fig. (2.7(a)), if the volume fraction increases, the particles arrange along the channel height in the same way: their distribution over the wall-normal direction is thus not directly driven by a change of ϕ. On the contrary, as shown in Fig. (2.7(b)) when the Reynolds number increases, the particles move to the center of the channel, thus pinching to a preferred position.

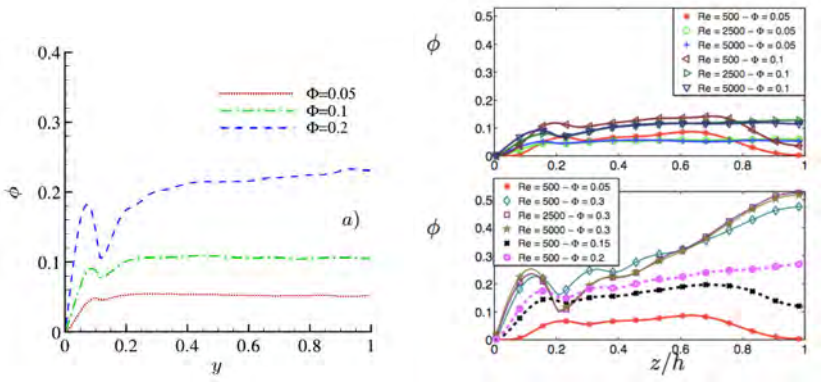

(a) (b)

Figure 2.7: Mean local volume fraction a) Picano et al. and b) I.Lashgari.

Picano et al. showed also that although the turbulent intensities are attenuated by the presence of a suspended part, the total drag, i.e. the friction Reynolds number (1.40) increases. In order to study the origin of this enhancement, they introduced the turbulent friction Reynolds number:

$$Re_T = \frac{U_\tau^T h}{\nu} \quad \text{where} \quad U_\tau^T = \sqrt{\frac{d\,\langle u_c' v_c' \rangle}{dy}} \tag{2.28}$$

While the friction Reynolds number Re_τ is a measure of the overall drag, the turbulent friction Reynolds number Re_T indicates only the portion of the drag directly introduced by the turbulent activity. These two Reynolds numbers were found to change differently when the volume fraction increases:

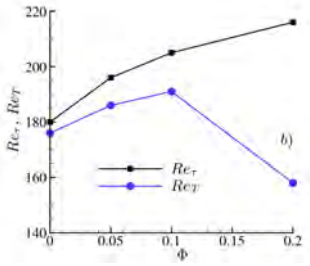

Figure 2.8: Friction Reynolds number and
turbulent friction Reynolds number (Picano et al.).

Fig. (2.8) shows that at high volume fractions there is an important reduction of Re_T. Picano et al. concluded that the drag enhancement was not linked to an increase of the turbulence activity but to the solid phase dynamics, and in particular to the increase of the particle-induced stress.

Two important non-dimensional parameters widely used for multi-phase flow analysis are the particle Stokes number St_p and the Bagnold number Ba, given respectively by:

$$St_p = \frac{\text{particle characteristic time}}{\text{fluid characteristic time}} = \left(\frac{d_p^2 \rho_p}{18\mu_f}\right) / \left(\frac{h}{u_b}\right) \tag{2.29}$$

$$Ba = \frac{\text{inertia stress}}{\text{viscous stress}} = \frac{\lambda^{1/2} \rho_p d_p^2 du/dy}{\mu_f} \tag{2.30}$$

where:

$$\lambda = \frac{1}{\left(\frac{\phi_0}{\phi}\right)^{1/3} - 1} \tag{2.31}$$

In Eq. (2.31) ϕ_0 is the maximal possible static volume fraction (which is equal to 0.74 for spherical particles) and ϕ is the actual volume fraction.

In his work Bagnold (see Bagnold, 1954) defined different regimes for the dense suspension flows studied:

-macro-viscous regime: in this regime, which appears below the value $Ba = 40$, the most important interactions are the particle-fluid interactions; moreover, Bagnold noticed that in this regime the shear rate varies linearly with the shear stress;

-grain-inertial regime: in this regime, which appears above the value $Ba = 450$, the most important interactions are the particle-particle interactions; in this case, Bagnold pointed out that the shear rate varies quadratically with the shear stress;

-transitional regime: between $Ba = 40$ and $Ba = 450$ the fluid is characterized by both particle-fluid and particle-particle interactions.

Using the definition of the bulk Reynolds number (1.28), it is possible to write the particle Stokes number and Bagnold number as follows (see Appendix A and B):

$$St_p = \left(\frac{d_p}{h}\right)^2 \frac{1}{18} Re_b R \tag{2.32}$$

$$Ba = 4\lambda^{1/2} \left(\frac{d_p}{h}\right)^2 Re_b R \tag{2.33}$$

where R is the ratio between the particle and the fluid densities.

In his experiments Bagnold deduced the values of Ba only by changing the volume fraction of the suspended phase. He was not able to judge the effects of the variation of other parameters. Starting from this remark and from Eq. (2.33), a big question arises: what happens to the flow if R varies? Are the Bagnold results valid even in this situation? Is the particle Stokes number important in this case?

Chapter 3

Methodology

This chapter is dedicated to the methodology used for solving fluid dynamics problems. The first part introduces the Computational Fluid Dynamics (CFD), the discipline whose aim is to solve numerically the equations governing a fluid in motion. The second part focuses on the Direct Numerical Simulations (DNS), and briefly describes the numerical code used for the present analysis. The latter were developed by W.P. Breugem at TU-Delft and is based on the Immersed Boundary Method. Every detail about the code can be found in Breugem's work, while a brief description extracted by this work is provided in this chapter for the sake of completeness.

3.1 Introduction to CFD

As already discussed, fluid dynamics problems are very complicated to treat. The unsimplified Navier-Stokes equations do not have any closed-form solution, so their resolution is possible only with mathematical methods. In particular, around a century of experience has shown that the turbulence problem is the most demanding to handle. Computational Fluid Dynamics is the discipline aimed to analyze and to solve the problems involving fluid flows with the aid of numerical methods and mathematical algorithms.

In all the possible approaches to the fluid dynamics equations, the procedure to solve them is the same:

-the first part, called the pre-processing part, involves the definition of the geometry, the discretization of the volume occupied by the fluid, the definition of the physical model and the setting of boundary conditions;

-the second part involves the simulations;

-the last part, called the post-processing part, involves the analysis and the presentation of the results.

There are many discretization methods available. The most used are:
-Finite Difference Method (FDM);
-Finite Volume Method (FVM);
-Finite Element Method (FEM).

The first method uses finite difference equations to approximate the derivatives. The other two methods involve the partition of the whole domain into simpler parts, called Finite Volumes or Finite Elements, and the calculation of the results at discrete places of these new sub-domains.

Physical modeling of turbulent problems represents another key tool in the CFD. The range of length-scales and the complexity of phenomena involved in turbulence make most of the modeling approaches prohibitively expensive. In some cases, the resolution required to solve all the scales involved in the turbulence and this is beyond what is computationally possible. The primary approach in such cases is to create numerical models to approximate the unresolved phenomena. The most used models are:

-RANS (Reynolds-Averaged Navier-Stokes equations): as already said in the first chapter, a flow velocity field can be decomposed in a mean (time-averaged) component and in a fluctuating component; the resulting Reynolds equations (Eq. (1.21a)-(1.21b)) can then be solved to determine the mean fluid velocity field. In this model, the Reynolds stresses are obtained from a turbulent-viscosity model and the turbulent viscosity is computed either through algebraic relations or through turbulent quantities such as the kinetic energy or the rate of dissipation;

-LES (Large Eddy Simulation): in this model, the smallest scales of the flow are removed through low-filtering operations: only the largest and most important scales of turbulence are kept into the filtered velocity field used for the resolution.

The third most common method in Computational Fluid Dynamics is the DNS (Direct Numerical Simulation): in this case, the Navier-Stokes equations are solved directly: all length-scale and time-scales are maintained and no hypothesis are made upon the velocity field.

As one may see from Fig. (3.1), the results obtained with these three methods are very different: in particular, the results obtained through a DNS are the most accurate, while the RANS ones are the most unsatisfactory (only the mean velocity field is shown). Nonetheless, the DNS simulations are the most computationally expensive, and sometimes the computational cost is too high for available computers. For this reason, RANS and above all LES algorithms are more used in applied problems, e.g. problems with high Reynolds number fluid flows.

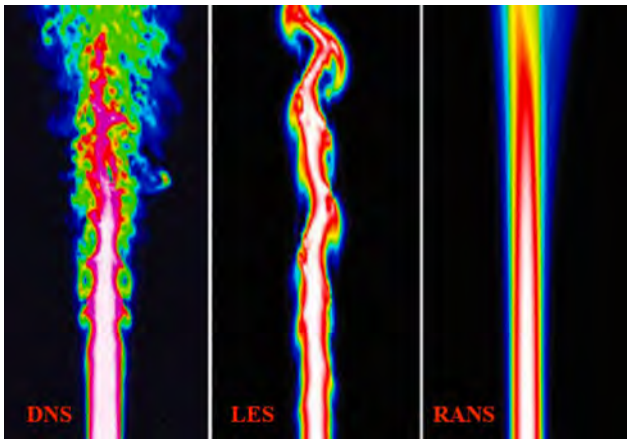

Figure 3.1: Difference in the results of a numerical simulation of a jet flow with DNS, LES and RANS approaches (ENEA).

Digital computers are used to perform the calculations. Given the nature of resolution methods, the more powerful the computer is, the fewer approximations can be made and the better the solution obtained results. Most of modern computers uses more than one processors to carry out their tasks. More than one calculation at the same time can be effectuated: the idea is then to reduce a single big problem into many smaller problems, solved simultaneously by different processors. Splitting a main task in many smaller tasks is called multithreading: the "master thread" is divided in various "slave thread", within the same processor. Multithreading programs have several advantages over single threading programs: better responsiveness to inputs, faster execution, lower resource consumption, better system utilization and simplified sharing and communication. The simultaneous resolution of single parts of a problem on different processors is called parallel computing: once the split of the master thread is done, the run-time system allocates the slave threads onto the available processors. Many different types of parallel computing can be employed. The most famous are: shared-memory multiprocessing (OpenMP) and distributed-memory multiprocessing (MPI); for the first case, the parallel processors have access to a common memory; for the second case, the parallel processors have their own memory and the informations are interchanged between processors through messages. Exactly as multithreading, parallel computing programs have many advantages over sequential computing programs, e.g. the drop of computational time. However, caution must be used: parallel computing programs are much more complicated to write than sequential ones and if the program is not perfectly written, many new bugs, such as in race conditions, can arise.

3.2 DNS of multi-phase flows

Let us focus on the method of the Direct Numerical Simulations (DNS) for the flow motion resolution. As already stated, a DNS consists in solving the Navier-Stokes equations with all the scales of motion. The level of description that they can reach is unrivaled, although their computational cost made them impossible to solve until the 1970s.

The large computational cost of a Direct Numerical Simulation is due to its high accuracy solution requirements. First of all, the domain size L must be large enough to represent the energy-containing motions and the grid spacing Δx must be small enough to resolve the dissipative scales. Moreover, the time step Δt must be limited in order to maintain a sufficient numerical accuracy. With respect to these parameters, the lowest and the biggest wavenumber represented in a DNS are:

$$k_{min} = 2\frac{\pi}{L} \tag{3.1a}$$

$$k_{max} = N\frac{\pi}{L} \tag{3.1b}$$

where N is the number of grid points: it is an indicator of the simulation size and consequently of the Reynolds number that can be attained.

Reasonable values for the above mentioned quantities L, Δx and Δt were found to be respectively:

$$L \approx 6.4/k_{min} \tag{3.2a}$$

$$\Delta x \approx 3.1/k_{max} \tag{3.2b}$$

$$\Delta t \approx \Delta x/20k_{max} \tag{3.2c}$$

The spacial requirements on the domain size and on the grid spacing determine the necessary number of grid nodes N^3 for a DNS, while the time requirement fixes the computational time T. Both can be expressed as functions of the Reynolds number as follows:

$$N^3 \propto Re^{9/4} \tag{3.3a}$$

$$T \propto Re^{11/4} \tag{3.3b}$$

Eq. (3.3a)-(3.3b) explain the reason why a DNS cannot be used for all the simulations. For high Reynolds number flows, the computational cost becomes too high for most of available computers. In these situations, it is necessary to reduce the computational time through a widening of the grid spacing. This leads to a diminution of the number of grid nodes and then of the computational time, but also to a deterioration of computed results, since in this case the smallest scales of motion are ignored.

Immersed Boundary Method

As already described in the previous chapter, when a second phase is added, the study of a flow and then its simulation becomes much more complicated. The mean difficulty of a multi-phase flow simulation arises from the coupling that has to be imposed between the the different phases of the flow. One of the most used method of two-phase coupling is the Immersed Boundary Method (IBM), firstly developed by Peskin (see Peskin, 1972).

In order to describe the IBM, let us refer again to the case of spherical particles suspended in a main fluid flow. The fluid phase is governed by the Navier-Stokes equations (1.9a)-(1.9b). For the solid phase, the velocity $\boldsymbol{u}^P$ of an infinitesimal particle segment at position x can be decomposed into a linear and an angular part:

$$\boldsymbol{u}^P = \boldsymbol{u}_c + \boldsymbol{\omega}_c \times \boldsymbol{r} \tag{3.4}$$

where $\boldsymbol{r} = \boldsymbol{x} - \boldsymbol{x}_c$ is the relative position to the particle centroid, $\boldsymbol{u}_c$ and $\boldsymbol{\omega}_c$ are the translational and the rotational velocities of the centroid, respectively. These velocities evolve according to the Newton-Euler Lagrangian equations, which for a sphere reduce to:

$$\rho_p V_p \frac{d\boldsymbol{u}_c}{dt} = \oint_{\partial V_P} \boldsymbol{\tau} \cdot \boldsymbol{n}\, dS + (\rho_p - \rho_f)\, V_p \boldsymbol{g} - V_p \nabla p_e + \boldsymbol{F}_c \tag{3.5a}$$

$$I_p \frac{d\boldsymbol{\omega}_c}{dt} = \rho_f \oint_{\partial V_P} \boldsymbol{r} \times \boldsymbol{\tau} \cdot \boldsymbol{n}\, dS + \boldsymbol{T}_c \tag{3.5b}$$

where ρ_p and ρ_f are the particle and the fluid densities, respectively, $V_P = 4\pi a^3/3$ is the particle volume, with a the value of the particle radius, $\tau = -p\boldsymbol{I} + 2\mu\boldsymbol{E}$ is the fluid stress, with $\boldsymbol{E} = \left(\boldsymbol{\nabla u}_f + \boldsymbol{\nabla u}_f^T\right)/2$ the deformation tensor, p_e is the contribution to the total pressure from a constant pressure gradient that can be imposed to drive a flow, $I_P = (2/5)\,\rho V_p a^2$ is the moment of inertia, $\boldsymbol{r}$ is the distance vector from the centroid of the sphere, $\boldsymbol{n}$ is the unity vector normal to the particle surface ∂V_p, and $\boldsymbol{F}_c$ and $\boldsymbol{T}_c$ are respectively the force and the torque acting on the particle as a result of collisions and physical contact with other particles or solid walls.

Unlike the other numerical methods, in a IBM the coupling between the fluid and the solid phase is not directly imposed through a no-slip/no-penetration condition, which would results in the following expression:

$$\boldsymbol{u} = \boldsymbol{u}^P(\boldsymbol{x}) \quad \forall \boldsymbol{x} \in \partial V \tag{3.6}$$

But instead, in the immediate vicinity of the particle a body force is added on the right-hand side of Eq. (1.9a), thus resulting on a good approximation of the above mentioned condition:

$$\frac{\partial \boldsymbol{u}}{\partial t} + \boldsymbol{u} \cdot \nabla \boldsymbol{u} = -\frac{1}{\rho}\nabla p + \nu \nabla^2 \boldsymbol{u} + \boldsymbol{f} \tag{3.7}$$

For a DNS, the solid and the fluid phases need to be followed through two different approaches: the Lagrangian approach for the particles (each single point of the particle is followed) and the Eulerian approach for the fluid (the whole field is followed as a unique entity). It is then necessary to use two different grids, a continuous Cartesian grid for the fluid phase (Eulerian grid) and an uniform grid attached to and moving with the surface of the particles (Lagrangian grid).

The IBM force $\boldsymbol{f}$ in Eq. (3.7) is computed in three steps:

1- Interpolation of a first prediction of the velocity from the Eulerian to the Lagrangian grid: this first step is carried out finding the index of the nearest Eulerian grid point to each Lagrangian grid point of the particle interface, then evaluating the velocities of all the Eulerian points within a preset neighborhood (two grid point in each direction), and finally calculating the Lagrangian grid point velocity through a regularized Dirac delta function;

2- Computation of the IBM force on the Lagrangian grid based on the difference between the interpolated first prediction of the velocity and the particle velocity;

3- Spreading of this force from the Lagrangian to the Eulerian grid.

The numerical code PARCHAN developed by W.P. Breugem

The numerical code adopted in the present thesis has been developed at TU-Delft by W.P. Breugem (see Breugem, 2012). The Navier-Stokes equations are solved using a second order finite-difference scheme associated to a direct-forcing IBM to couple fluid and solid phases. Short-range interactions occurring below the mesh size are considered using lubrication corrections and a soft-sphere collision model. The main feature of the present algorithm is that it can achieve a global second order accuracy in space. The numerical code were validated in several studies where test cases can be found, e.g. [9], [26]. The algorithm is coded in Fortran using both OpenMP and MPI paralleling methods in order to reduce the computational time and the memory utilization. The calculations are set to be carried out through parallel computing on multi-processor machines with distributed memory.

Chapter 4

Results

This last chapter is dedicated to the discussion of the results obtained by the Direct Numerical Simulations carried out during this project. In the first section the set-up of the simulations is fully described. In the second section the results are shown with the following order: first of all a comparison between the different regimes detected through the simulations is displayed. Thereafter each of the two regimes is separately analyzed: firstly the so-called hydrodynamic regime and secondly the so-called ballistic regime. The last part focuses on the analysis of the results through the non-dimensional parameters normally used to describe the multi-phase flows: the particle Stokes number and the Bagnold number.

4.1 Simulation Set-up

The case studied in this work is a pressure driven channel flow developing between two infinite flat walls located at $y = 0$ and $y = 2h$. With reference to Fig. (4.1(a))-(4.1(c)), the domain sizes are $L_x = 6h$, $L_y = 2h$ and $L_z = 3h$ in the streamwise, wall-normal and spanwise directions, respectively. Periodic boundary conditions are imposed in in the streamwise, x, and spanwise, z, directions. A mean pressure gradient acting in the streamwise direction imposes a fixed value of the bulk velocity u_b across the channel, which leads to a constant value of the bulk Reynolds number: $Re_b = u_b\, 2h/\nu = 5600$. This value of the bulk Reynolds number corresponds to a friction Reynolds number equal to $Re_\tau = u_\tau h/\nu = 180$ for the single phase case ($u_\tau = \sqrt{\tau_w/\rho}$ the friction velocity). Gravity and buoyancy effects are neglected in this study to focus only on the inertial effects of different density ratios. It should be noted however that at sufficiently high velocity buoyancy effects become negligible with respect to inertial dynamics (high Froude number).

The domain is discretized by a cubic mesh of 864 x 288 x 432 point in the streamwise, wall-normal and spanwise directions. The typical mesh size is of the order of the viscous and Kolmogorov lengths. Non-Brownian spherical rigid particles are considered. The value of their radius is fixed to the channel half-width value, given by $a/h = 18$. The particle radius a spans about 8 points of the Eulerian mesh which corresponds to around 800 points used to discretize the particle surface in the Lagrangian frame.

The following simulations have been carried out:

Volume Fraction ϕ	0.05	0.02	0.002
Number of particles N_p	2500	1000	100
Density Ratios R	1, 2, 4, 10, 100, 1000	100	100
Domain Sizes L_x L_y L_z	$6h \times 2h \times 3h$		
Mesh Points N_x N_y N_z	$864 \times 288 \times 432$		

Table 4.1: Summary of the Direct Numerical Simulations reported in this work. The number of particles is given by $N_p = \frac{6\phi L_x L_y L_z}{\pi}$, where L_x, L_y and L_z are the domain sizes.

The simulations with $\phi = 0.05$ start from a turbulent and statistically stationary regime for the particle-laden flow with unitary ratio between particle and flow densities (see Picano et al., 2015). The new density ratio is then imposed and the statistics are collected after the transient phase. The simulations with $\phi \neq 0.05$ start instead from a turbulent and statistically stationary regime for the flow phase without any particle. The new volume fraction as well as the new density ratio is then set and the statistics are collected again once the statistically stationary regime is reached.

All the simulations have been performed using 576 cores of a CRAY XE6 supercomputer LINDGREN hosted at the Center for High Performance Computing, PDC, KTH, Stockholm. Each simulation needed around 100.000 core-hours to obtain enough samples of the statistical steady regime in order to have convergent statistics.

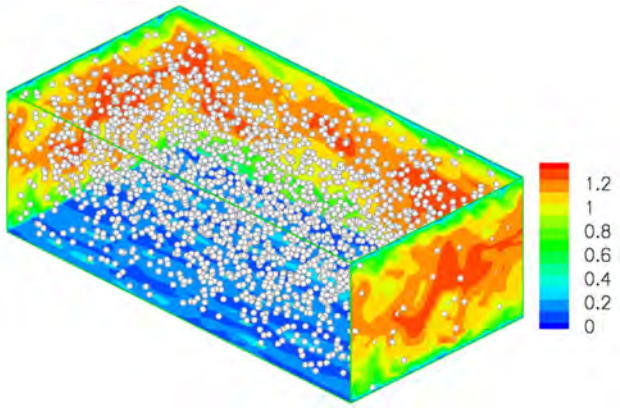

(a)

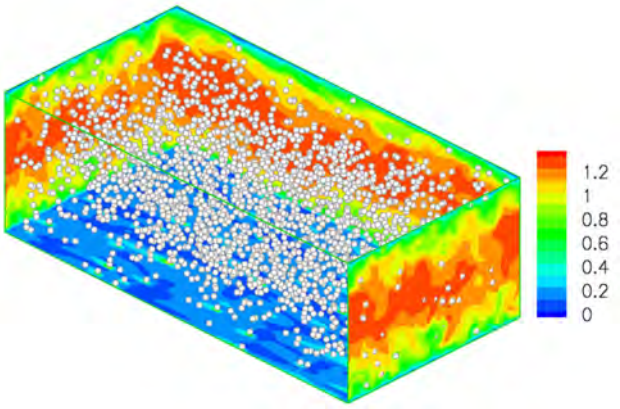

(b)

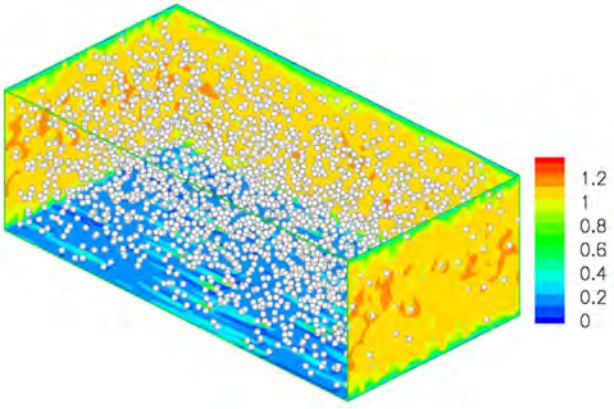

(c)

Figure 4.1: Snapshot of the streamwise velocity on different orthogonal planes together with the particle distribution for $\phi = 0.05$ and a) $R = 1$, b) $R = 10$ and c) $R = 100$. All the datas for these figures were collected in the statistically stationary regime.

4.2 Results

For all the cases above mentioned, the study focused on the velocity statistics, for both phases, and on the single-point dispersions, for the solid phase.

Velocitiy Statistics

As already analyzed in Section (1.4), the velocity of a fluid in motion can be decomposed in a mean term $U_i(x_i, t)$ and in a fluctuations term $u_i'(x_i, t)$. Through the investigation of their statistics it is possible to understand how the different parameters affect the mean flow behavior, the turbulent activity and where, along the height of the channel, this activity is more important.

Dispersions

The analysis of the dispersions, i.e. the average displacements of the particles from their initial positions, allows to study how the particles move and spread around the channel. Moreover, from their profiles it is possible to deduce the so-called correlation time, i.e. the time at which the actual value of the velocity has no longer relation with the initial value.

According to Taylor (see Taylor, 1922), it is possible to express the displacement of a particle along a general i direction through a series:

$$x_i(t) - x_i(0) = v_i t + \mathcal{O}(t^2) \tag{4.1}$$

Within the neighborhood of $t = 0$ it is possible to neglect the value of the $\mathcal{O}(t^2)$, while this approximation for longtime behaviors is no longer valid. Investigating the mean square value of the displacement (MSD), Taylor obtained the following expression:

$$\left\langle |x_i(t) - x_i(0)|^2 \right\rangle = \begin{cases} \sigma_u^2 t^2 & t \ll T_L \quad (4.2a) \\ 2\sigma_u^2 T_L t & t \gg T_L \quad (4.2b) \end{cases}$$

where σ_u is the variance of the velocity and T_L is the correlation time: after this time T_L the approximation to the first order of Eq.(4.1) is not valid anymore.

The above system can be simplified using the so-called diffusion coefficient D_t:

$$D_t(t) = \begin{cases} \sigma_u^2 t & t \ll T_L \quad (4.3a) \\ \sigma_u^2 T_L & t \gg T_L \quad (4.3b) \end{cases}$$

Thus, in the neighborhood of $t = 0$, the MSD is proportional to the square of t, while after T_L the MSD varies linearly with t.

4.2.1 Hydrodynamic regime vs Ballistic regime

The snapshots of Fig. (4.1) presented the streamwise velocity displayed in some orthogonal planes together with the particle position. The cases at $R = 1$ and $R = 10$ showed the typical turbulent behavior with high level of fluctuations and velocity streaks close to the wall. On the contrary at $R = 100$ the velocity field is almost uniform with a low level of fluctuations. This strong change suggests the appearance of a new regime when the particle density is high enough. These aspects are discussed in the present section.

Velocity Statistics

Let us firstly the case shown in Fig. (4.2(a))-(4.2(d)) of the channel flow at $\phi = 0.05$, with the density ratio increasing from $R = 1$ to $R = 1000$.

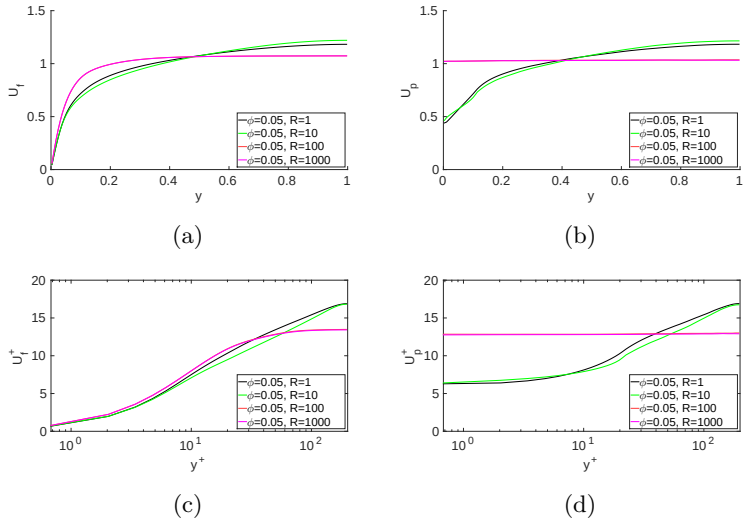

Figure 4.2: Mean fluid velocities in a) outer units and c) inner units and mean particle velocities in b) outer units and d) inner units.

At density ratio $R = 1 \div 10$, the presence of the particles weakly alters the mean velocity profile which is similar to that of the single-phase flows. It displays the usual linear viscous sub-layer Eq. (1.44) ($U^+ \simeq y^+$) at $y^+ < 5$ and the log-law Eq. (1.45) ($U^+ = (1/k)log(y^+) + B$) at $y^+ > 40$. The particles tend in mean to move with the flow apart from the first layer of particles close to the wall which shows higher velocity with respect to the flow. Actually, these are friction-less particles that can slide on the wall so this situation is expected. On the other hand, above a certain value

of density ratio ($R \geq 100$), the situation radically changes: the particles move along the streamwise direction with a uniform nearly-constant velocity and the correspondent mean fluid velocity approaches the profiles of the so-called plug-flows in the bulk region. The log-layer region completely disappears suggesting a very different behavior with respect to the usual turbulent channel single-phase flow. We will refer to the former case as "hydrodynamic regime", where particles and fluid still mutually interact and the overall behavior is still similar to the unladen case. We will refer to the second case as "ballistic regime" instead, in which the particles owing a high inertia do not "feel" anymore the presence of the fluid and where the leading interactions are the particle-particle collisions.

A further confirm of the previous behavior can be found in the fluctuating velocity statistics, both for the fluid phase in Fig. (4.3(a))-(4.3(e)) and for the solid phase in Fig. (4.4(a))-(4.4(e)).

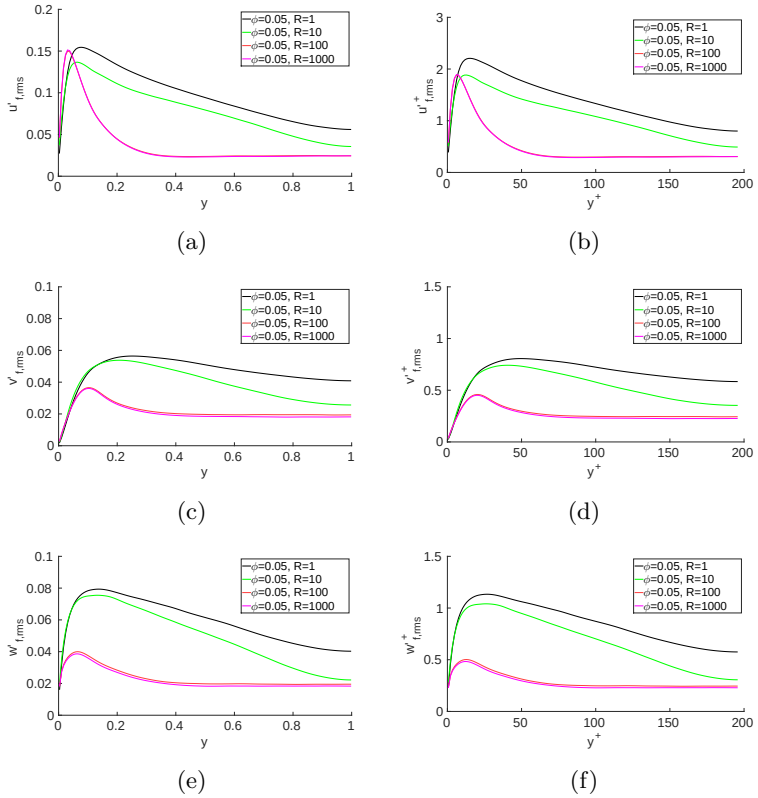

Figure 4.3: Intensity of the fluctuation velocity components for the fluid phase in a), c), e) outer units and b), d), f) inner units.

These figures show that while in the hydrodynamic regime the fluctuating velocities are influenced by the changes of the density ratio value, in the ballistic regime the increase of the particle density does not affect their behavior. Moreover, the fluctuating velocity profiles are completely different in the two cases: while in the hydrodynamic regime the fluctuations change over the height of the channel, in the ballistic regime they are almost constant and have similar values in the three directions. This behavior confirms that the large inertia of the particles with high R make the move ballistically similar to the molecules of a dilute gas. This regime does not depend anymore on R since the particles do not feel the fluid flow, though they affect the whole flow behavior. In the hydrodynamic regime instead since the two phases mutually interact the change of R alters the flow dynamics.

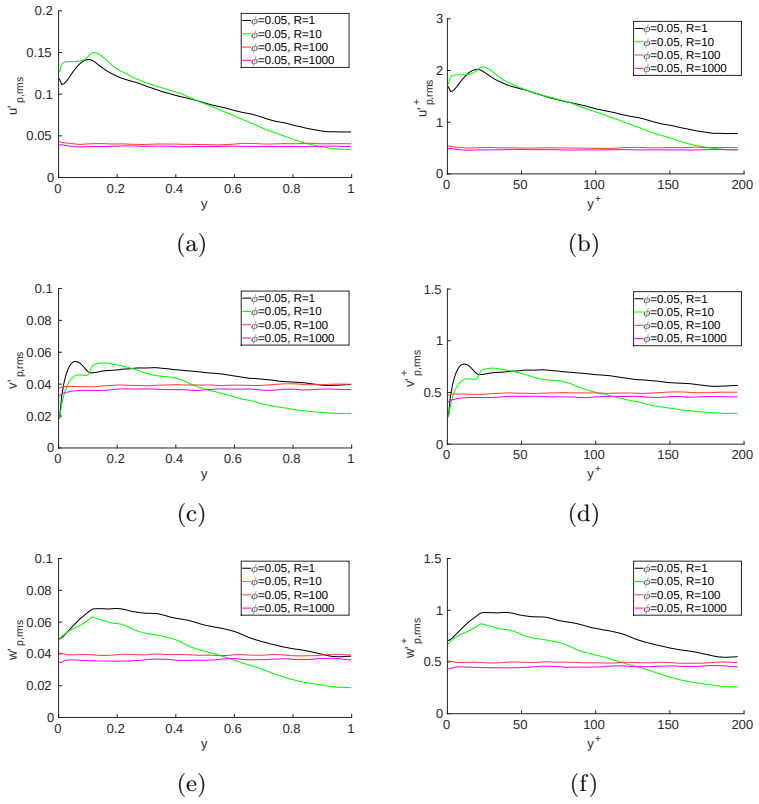

Figure 4.4: Intensity of the fluctuation velocity components for the solid phase in a), c), e) outer units and b), d), f) inner units.

All the velocity statistics here briefly explained are studied and analyzed more in-depth in next sections for each of the two regimes, in order to better understand how the change of the particle properties affects the flow.

Dispersions

As last statistics to show the important differences between the two regimes, the particle dispersion is here reported in the streamwise direction measured as the mean square displacement of the streamwise particle position subtracted of the mean displacement, $\langle \Delta x_p^2 \rangle$. As shown in Fig. (4.5) the dispersion of the particles in the hydrodynamic regime is much more effective than in the ballistic regime. The wall-normal inhomogeneity and the turbulent fluctuations are much more effective to mix the particles during their motion. On the contrary the flat mean velocity of the particles together with the low and flat velocity fluctuations of the ballistic regime make the particles moving as a plug flow without mix.

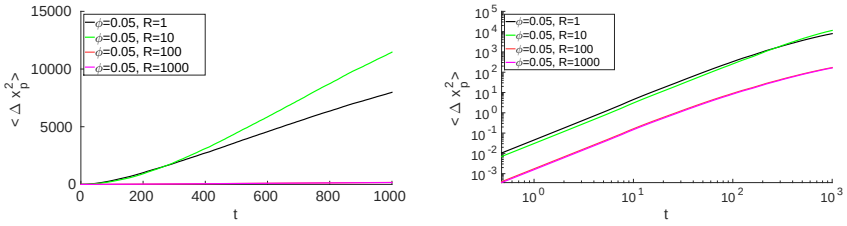

Figure 4.5: Mean square fluctuating displacement $\langle \Delta x_p'^2 \rangle(t)$ vs t.

.

More details about these aspects of the dispersions will be presented in the section of the specific regimes.

4.2.2 Hydrodynamic regime

Velocity Statistics

Let us now focus on the so-called hydrodynamic regime. Four cases are here analyzed: $R = 1, 2, 4, 10$, all of them at $\phi = 0.05$ considering 2500 particles in the computational domain.

As one can see from Fig. (4.6), changing the value of the density ratio has a small impact on the properties of the flow. It appears that a change even by one order of magnitude of the density ratio R and in turns in the mass fraction $M = R\phi$ does not produce significant effects. This leads to the conclusion that in the hydrodynamic regime the changes in the overall properties are driven by the changes in the values of the volume fraction (see Picano et al., 2015) rather than in the values of the density ratio.

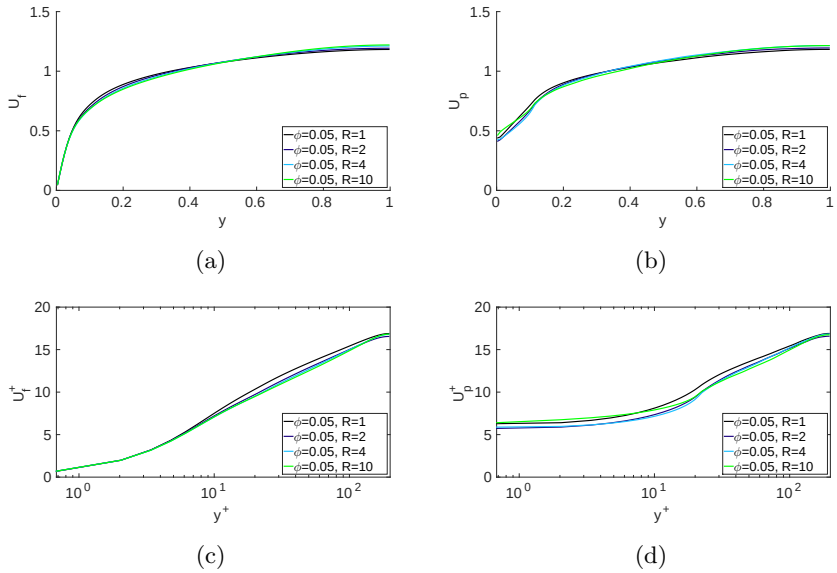

Figure 4.6: Mean fluid velocities in a) outer units and c) inner units and mean particle velocities in b) outer units and d) inner units.

A very interesting result for these cases were obtained with the analysis of the particle distribution on the wall-normal direction, see Fig. (4.7).

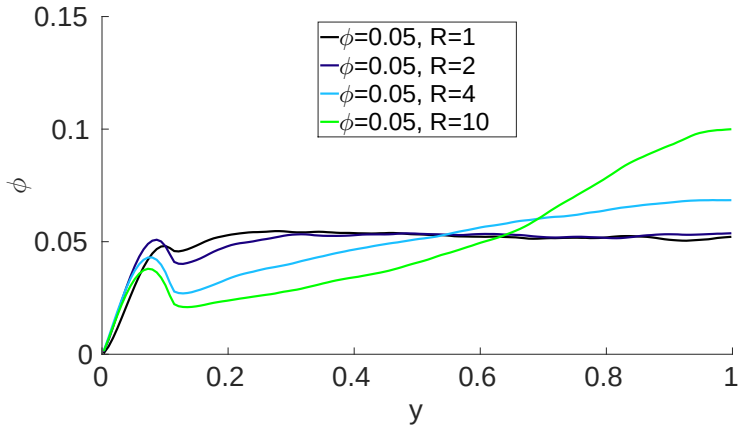

Figure 4.7: Mean local volume fraction as a function of the wall-normal position.

When the density of the solid phase increases, the particles tend to move toward the centre of the channel. This behavior is due to a combination of shear-induced and inertial migrations. A similar behavior has been found

for much denser suspensions at $\phi = 0.3$ of neutrally buoyant particles, see Fig.(2.7(a)) . The inertial shear-induced migration can be phenomenologically interpreted considering the high collision rate occurring among non aligned particles in high shear region. The collided particles result scattered away in the shear direction creating a mean drift. The large particle inertia of high R induces an enhanced collision rate which probably becomes similar to that of denser cases with $R = 1$ where these effects have been observed.

Let us now focus on the intensity of the fluctuating velocities in the hydrodynamic regime, both for the fluid phase in Fig. (4.8(a))-(4.8(e)) and for the solid phase in Fig. (4.9(a))-(4.9(e)).

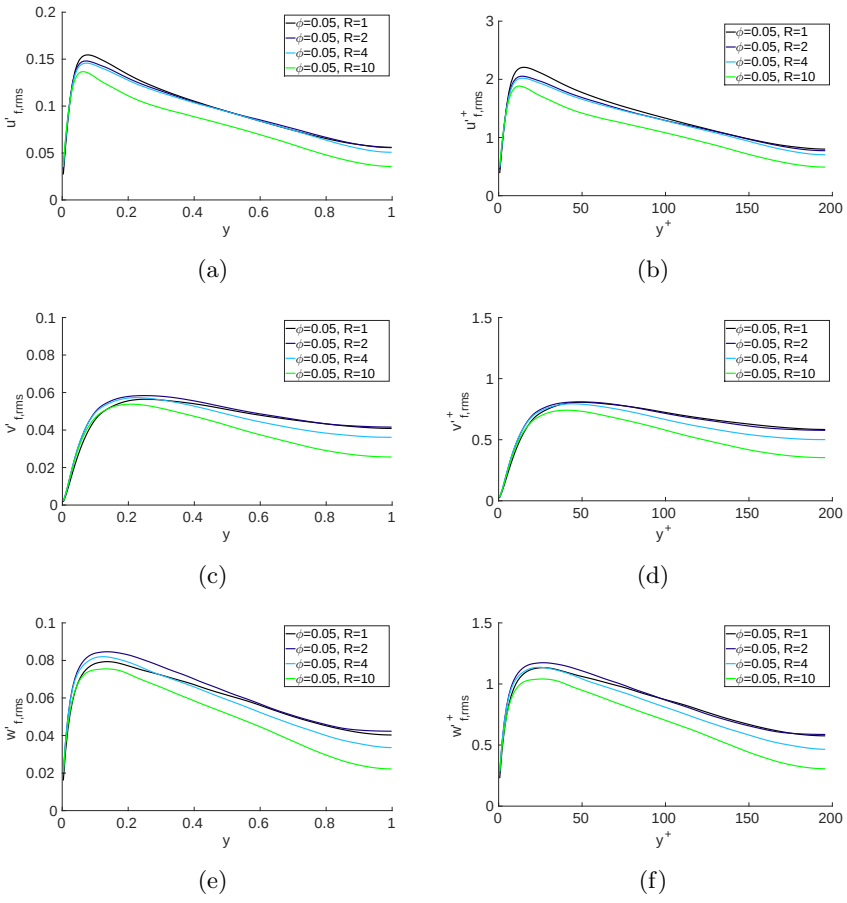

Figure 4.8: Intensity of the fluctuation velocity components for the fluid phase in a), c), e) outer units and b), d), f) inner units.

The increase of the density ratio usually leads to a diminution of the turbulence activity. In particular, the intensity of the first peak of the

fluid turbulent intensities near the wall is reduced. Beyond this region, the diminution of the turbulent activity follows a similar path for the rest of the channel for all the components reaching also a 20% of reduction at $R = 10$. Once again, it is interesting to notice that the diminutions of the turbulence activity are less important than them found when changing the volume fraction of a factor 2-4, meaning that the reduction of the turbulence is driven more by the changes in the value of the volume fraction rather than by the changes in the value of the density ratio. The particle velocity fluctuation intensities show a similar behavior with the exception of the near wall region where the increase of R can lead to a growth of the fluctuation level. This can be attributed to the higher momentum induced by the larger inertia of the particles reaching the wall from the bulk of the flow.

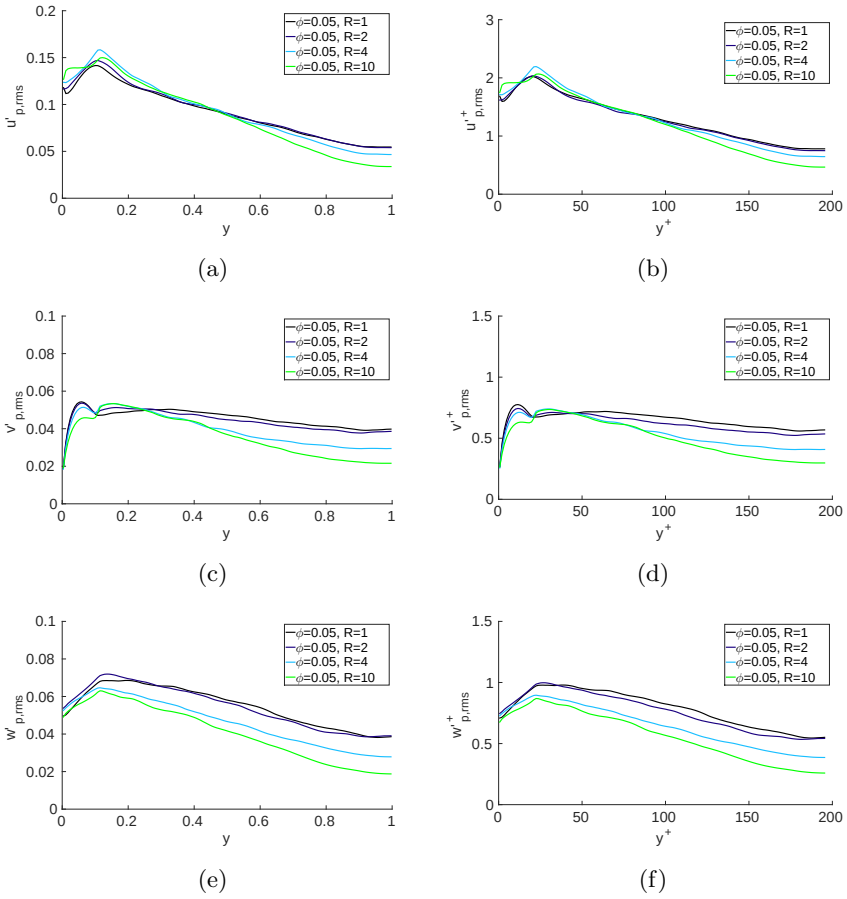

Figure 4.9: Intensity of the fluctuation velocity components for the solid phase in a), c), e) outer units and b), d), f) inner units.

Dispersions

Let us now focus on the different profiles of the mean square displacement fluctuations for the cases with $\phi = 0.05$ and R increasing from 1 up to 10.

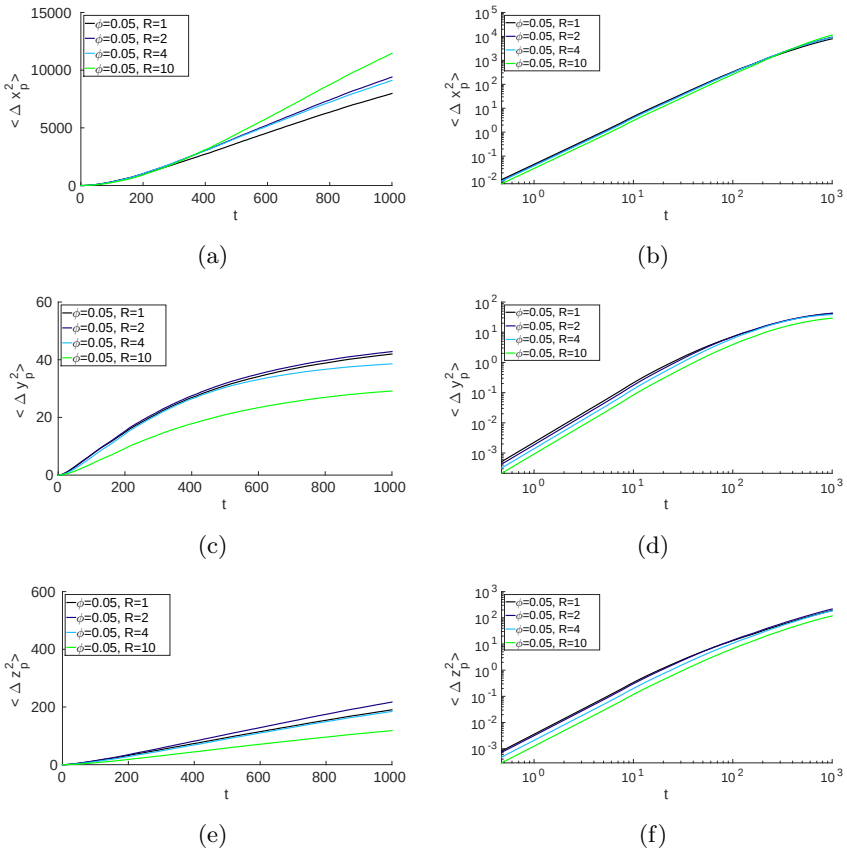

Figure 4.10: Dispersion on a), b) streamwise, c), d) wall-normal and e), f) spanwise directions.

As one can see from Fig. (4.10(b)), (4.10(d)) and (4.10(f)), the density ratio does not affect significantly the mean square displacement fluctuations in log-log plots. This means that the general dispersion mechanisms remain unaltered with small difference in the correlation time scale T_L and in the diffusion coefficient D_t. These aspects are not unexpected given the similar level of velocity fluctuation intensities shared by the cases at different R. Nonetheless, looking to the same plots in linear scale allow to discern more easily the differences. An anisotropic behavior of the dispersion rate for the three directions changing R can be observed: while the streamwise mean

square displacement fluctuation $\langle \Delta x'^2 \rangle$ is larger increasing R, the other two components reduce. These aspects are associated to the diffusive uncorrelated dynamics, resulting in different diffusion coefficients $D_{t,i}$. The diffusion coefficient results almost the double at $R = 10$ than $R = 1$ in the streamwise direction, while it is the half in the spanwise direction. It should be noted that the wall-normal mean square displacement will always saturate given the fixed distance between the walls. In other words at high R particles tend to separate more in the streamwise direction than in the transversal ones.

4.2.3 Ballistic regime

Velocity Statistics

Let us now consider the so-called ballistic regime. Four cases are analyzed: two cases with $\phi = 0.05$ and $R = 100, 1000$ and two cases at $R = 100$ with $\phi = 0.02$ and $\phi = 0.002$.

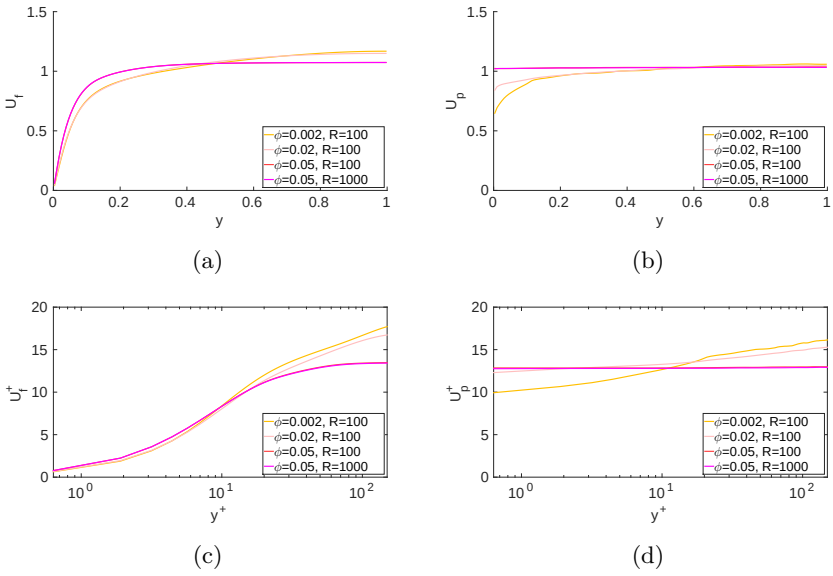

Figure 4.11: Mean fluid velocities in a) outer units and c) inner units and mean particle velocities in b) outer units and d) inner units.

As one can see from Fig. (4.11(b))-(4.11(d)), the mean velocity of the particles is more or less constant for all the four cases along the streamwise direction. The differences with respect to the mean value for the dilute cases at $\phi = 0.02$ and $\phi = 0.002$ are negligible after the first particle layer

at the wall and however, everywhere lower than the 20% of the mean value of the velocity. The mean fluid velocity profiles of these dilute cases (Fig. (4.11(a))-(4.11(c))) are less interesting: the small amount of particles involved on the simulations for the cases with $\phi = 0.02$ and $\phi = 0.002$ is not able to affect the properties of the fluid. The mean value of the fluid velocity is then only slightly altered by the presence of the particles. It should be remarked however that though quite dilute in volume fractions, these cases still have high mass fraction $M = R\phi$, so it is not completely expected a small effect on the flow statistics. The case at $\phi = 0.05$ is different, since presents a plateaux in the bulk region, typical of a plug flow. In this central region the flow behaves more as a solid without a mean shear. The high inertia of the particles tend to froze the suspension.

The particle average distribution is shown in Fig. (4.12). In this case, the mean local volume fraction has been divided by the number of the particles, in order to have an effective comparison of the particle distribution along the wall-normal direction for the different cases. This figure clearly shows that in the ballistic regime the particles spread along the height of the channel in the same way, for all the cases without showing anymore any preferential concentration.

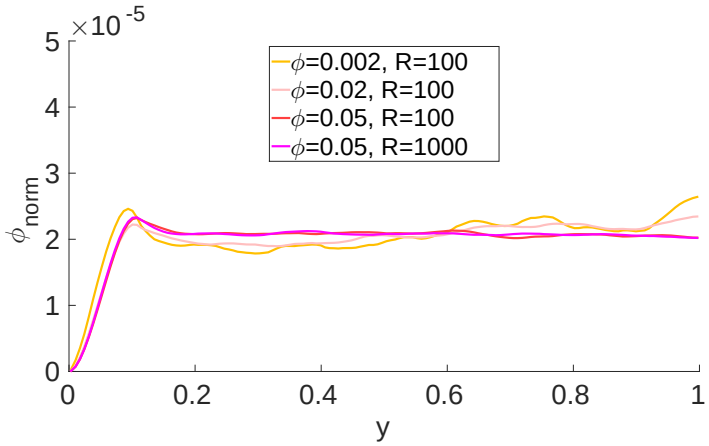

Figure 4.12: Mean local volume fraction as a function of the wall-normal position normalized by the number of particles.

Let us now consider the intensities of the fluctuating velocities, both for the fluid phase in Fig. (4.13(a))-(4.13(e)) and for the solid phase in Fig. (4.14(a))-(4.14(e)).

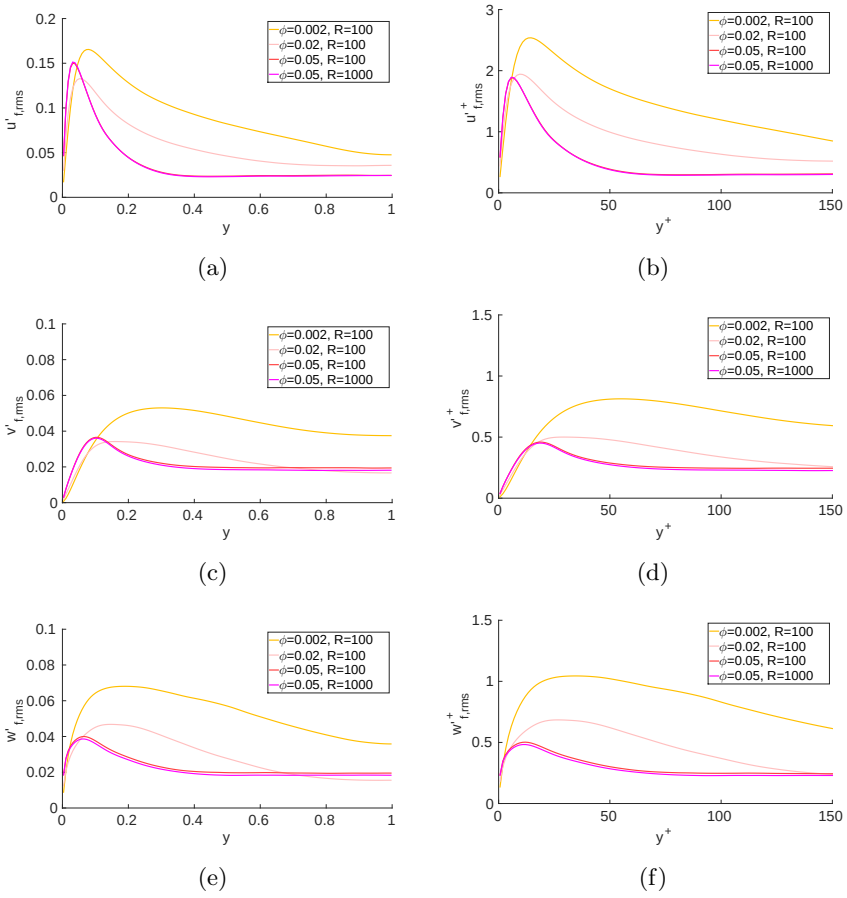

Figure 4.13: Intensity of the fluctuation velocity components for the fluid phase in a), c), e) outer units and b), d), f) inner units.

In all the cases there is an important turbulent activity near the wall. Differently of the mean field, Fig. (4.13(a))-(4.13(f)) show that the presence of few dense particles can alter the turbulent dynamics. A first reduction of the turbulent intensities is seen starting from the case with $\phi = 0.02$, which tends toward the trends already analyzed of the cases with $\phi = 0.05$, where all the three components of the turbulent intensity presented an almost constant value. At $\phi = 0.05$ the fluctuations intensities of the particle velocity are constant and almost identical for each component being equal to that of the fluid phase in the bulk region. The particles behave as a dense gas with isotropic velocity fluctuations. The dilute cases at $R = 100$ show some differences. The streamwise particle velocity fluctuation tends to be higher than the corresponding quantity for the fluid phase, while the oppo-

site occurs for the other components. The particle velocity dynamics of these dilute cases seems to be coupled with the mean motion which is a source for the streamwise velocity fluctuation. This mechanics induces higher fluctuations in the streamwise then in the transversal directions. When the particle concentration increases, the collisions start to dominate and tend to equally distribute the kinetic energy of the particles. In other words, at high R the particle dynamics is weakly affected by the motion of the fluid phase and feels only the mean flow behavior. When the concentration is high enough a collision dominated regime occurs. The collision tend to equally distribute the particles and their kinetic energy.

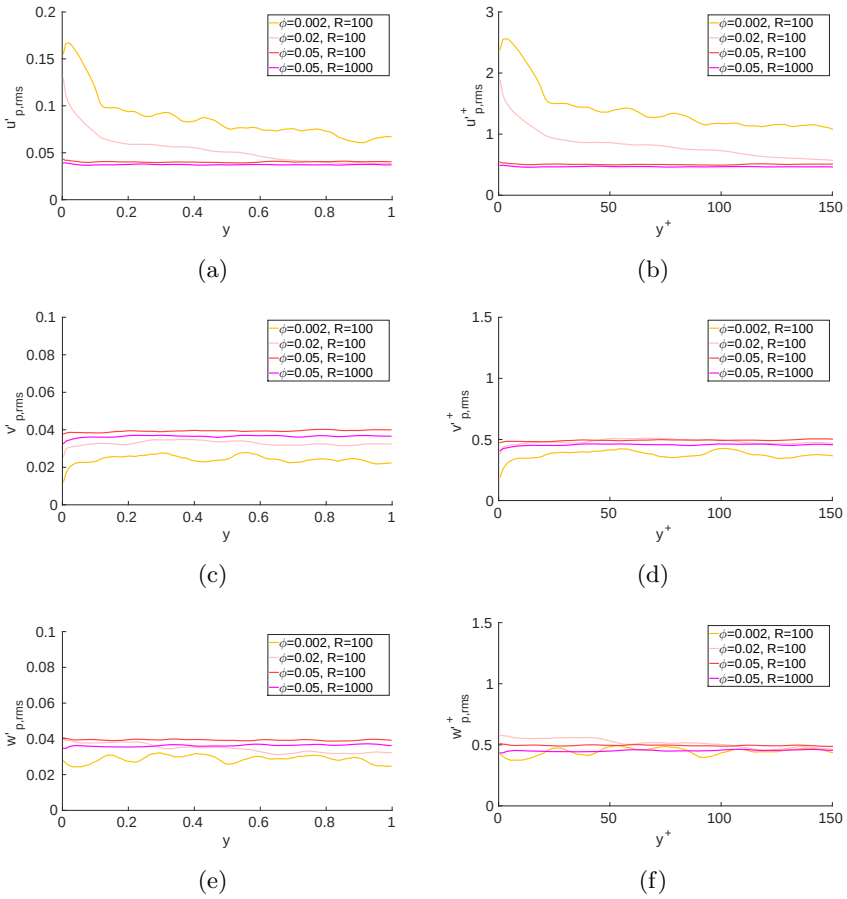

Figure 4.14: Intensity of the fluctuation velocity components for the solid phase in a), c), e) outer units and b), d), f) inner units.

Dispersions

Let us now focus on the different profiles of the mean square fluctuating displacements for the four cases of ballistic regime above mentioned.

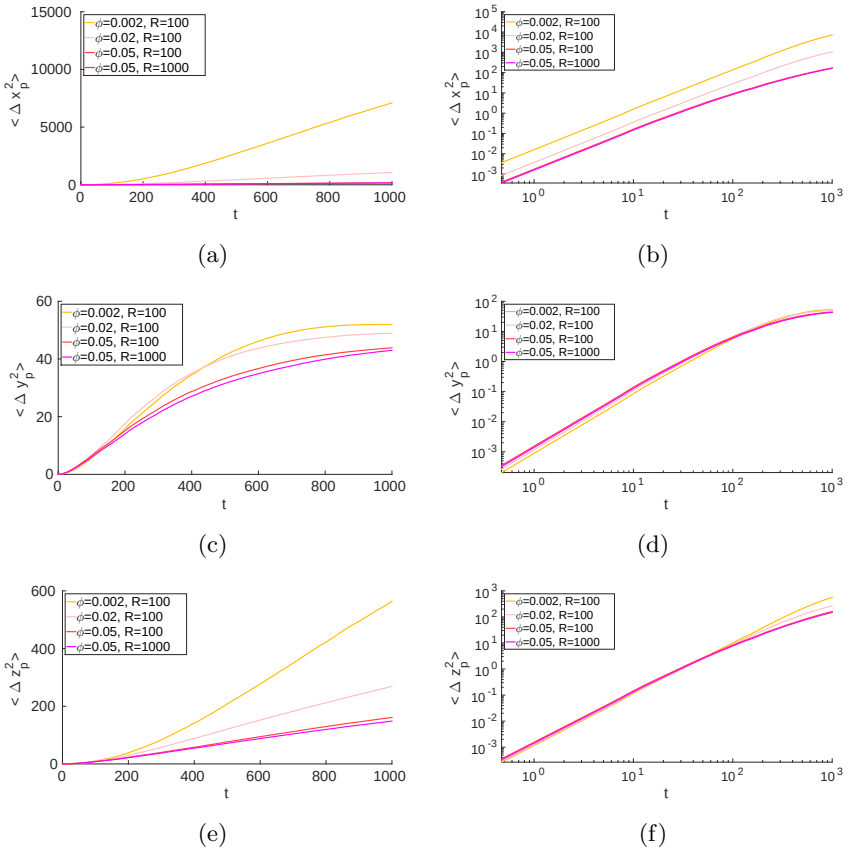

Figure 4.15: Dispersion on a), b) streamwise, c), d) wall-normal and e), f) spanwise directions.

In the ballistic regime, the diffusion phenomenon seems to evolve differently to the other cases. As easily expected, in the case of $\phi = 0.002$, the few particles are more "free" to move, so they tend to drift apart from their starting point more than the other cases. However, it seems that in this case the correlation time is bigger, meaning that the particle velocities are correlated to the initial values longer for the dilute cases than the others cases. This can be explained with the higher freedom that they have in their motion, leading to a reduced probability of collisions with the other particles moving in the channel.

4.3 Total stress balance

In order to better understand the momentum exchange between the fluid and the solid phase in dense suspensions, the streamwise momentum budget was examined. Following the rationale on the mean momentum budget given in Appendix C, it is possible to write the whole budget as a sum of three terms:

$$\tau = \tau_V + \tau_T + \tau_P \tag{4.4}$$

where $\tau = u_\tau^2(1-y)$ is the total stress, $\tau_V = \nu(1-\phi)(dU_f/dy)$ is the viscous stress, $\tau_T = -\langle u_c' v_c' \rangle$ is the turbulent Reynolds shear stress ($\langle u_c' v_c' \rangle = R\phi\langle u_p' v_p' \rangle + (1-\phi)\langle u_f' v_f' \rangle$, with the terms on the right hand side representing the particle Reynolds stress and the fluid Reynolds stress, respectively) and $\tau_P = (\phi/\rho)(\langle \sigma_{p,xy} \rangle)$ the particle induced stress.

The coefficient R is source of numerical issues: the statistical noise arising from the results of the simulations is amplified by R; this would require a computation much longer than in the other cases. For this reason, only the mean value of the stresses is here reported, as a function of R.

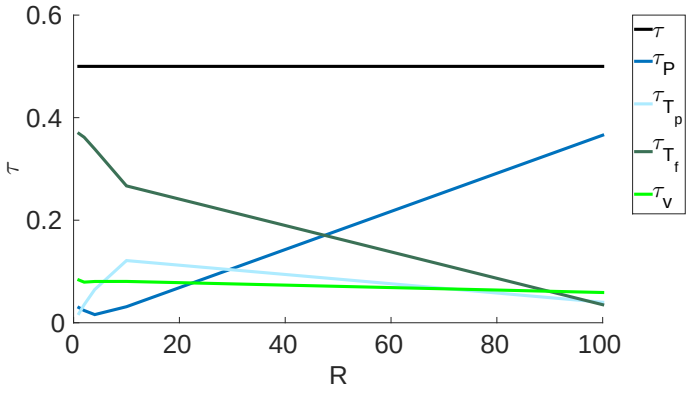

Figure 4.16: Momentum budget for different density ratio R at $\phi = 0.05$. All the values are averaged along the height of the channel.

From Fig. (4.16) it seems that the results obtained by Picano et al. can be extended also when the volume fraction is fixed and R is increased. When the value of the density ratio (and then of the mass fraction) is increased, the viscous stress is almost constant, and the particle induced stress enhances. Interestingly, while in the hydrodynamic regime the particle Reynolds stress increases until $R = 10$, in the ballistic regime the fluid and the particle Reynolds stress decreases with R and the particle stress increases becoming the leading term. This demonstrate that the hydrodynamics regime is con-

trolled by the turbulence with the particles affecting this regime mainly via the solid phase Reynolds stress: the particles transport a large amount of momentum with their correlated turbulent motions. In the ballistic regime instead Fig. (4.16) shows the dominance of the particle stress similarly as discussed by Lashgari (see Lashgari et al., 2014) for high ϕ at $R = 1$.

4.4 Interpretation

Using the definitions of Eq. (2.30), (2.29) and (1.40), for the simulations above described the following values were found:

$Case$	Ba	St_p	Re_τ
$\phi = 0.05, R = 1$	115	1.92	196
$\phi = 0.05, R = 2$	229	3.84	201
$\phi = 0.05, R = 4$	458	7.68	202
$\phi = 0.05, R = 10$	1 146	19.20	203
$\phi = 0.05, R = 100$	11 462	192.04	223
$\phi = 0.05, R = 1000$	114 628	1920.4	224
$\phi = 0.002, R = 100$	5 562	192.04	183
$\phi = 0.02, R = 100$	9 054	192.04	191

Table 4.2: Values of the Bagnold number, the particle Stokes number and the friction Reynolds number for all the cases studied.

In his work, Bagnold stated that his non-dimensional parameter was able to describe the transition from the hydrodynamic to the 'grain dominated' regimes and he found that this transition appeared between $Ba = 40$ and $Ba = 450$. As one can see from Table (4.2), the situation is now different. In his work Bagnold did not investigated the behavior of the suspension when the density ratio changes, while his theory has been proven several time at fixed R and changing ϕ and Re_τ. The results of Table (4.2) clearly show that the values found by Bagnold are not anymore valid in this case.

At the same time the Stokes number, which is the other parameter normally used for the description of the particle dynamics in dilute particle-laden flows, seems not to completely describe the transition between the hydrodynamic and the ballistic regimes. On one hand, when the particle Stokes number $St_p > 100$, it was found that the particle dynamics tend to be uncoupled with the fluid phase dynamics, so it seems to give a criterion to discern these situations. However, the particle Stokes number does not take into account the changes in the values of the volume fraction of the dispersed phase. For this reason, since different values of the volume fraction were found to lead to very different flow behavior (see for example Fig. (4.11(b)) and (4.14(b))), with these datas it is possible to conclude that the Stokes number alone cannot describe the transition.

In order to show that the Bagnold number does not well describe the transition between the hydrodynamic and the ballistic regimes for the cases reported in this work, the effective viscosity has been calculated as a function of the Bagnold number and has been compared to the same function when the volume fraction is increased. This quantity should increase linearly with Ba in the particle dominated regimes following the Bagnold theory.

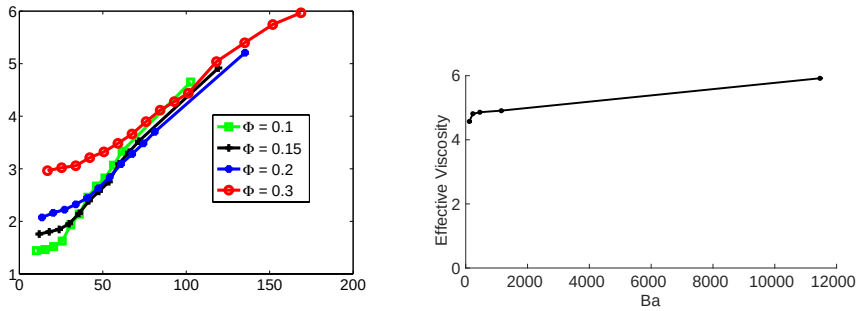

(a) (b)

Figure 4.17: Effective viscosity
a) for different bulk volume fractions ϕ and $R = 1$ (courtesy of Iman Lashgari) and b) for different density ratios R.

While in Fig. (4.17(a)) fixing $R = 1$ the effective viscosity approached a linear dependance with Ba at sufficiently high Bagnold number (exactly as described by Bagnold), in Fig. (4.17(b)) there are not such dependences anymore. It is then possible to conclude that the Bagnold number does not describe the transition from the hydrodynamic to the ballistic regimes when R is changed.

Conclusions

This Master thesis project focused on the study of a turbulent channel flow laden with finite-size particles at relatively high volume fractions ϕ and different solid to fluid density ratios R. The direct numerical simulations reported in this work were performed by a parallel code developed by W.P. Breugem at TU-Delft (see Breugem, 2012), using 576 cores of the CRAY Supercomputer LINDGREN at PDC, KTH, Stockholm. The coupling between the fluid and the solid phases was set through an Immersed Boundary Method. The aim of the present work was to clarify the effect of the density ratio R on the suspension dynamics. The bulk Reynolds number has been kept constant at $Re = 5600$ and the volume fraction has been initially set to $\phi = 0.05$, with the density ratio increasing from $R = 1$ to $R = 1000$. The results suggested to test suspensions at lower volume fractions ($\phi = 0.002$ and $\phi = 0.02$) with high particle density.

Two different flow regimes were detected. As long as the density ratio remains under a certain value ($\sim$10), we observe a regime where the fluid-particle interactions and the particle-particle interactions drive together the flow behavior. In this "hydrodynamic" regime the enhancement of the particle density tends to slight decrease the turbulence activity. The dynamics remains similar to that of the single-phase flows with some small differences. An interesting aspect of this regime is the inertial migration towards the center of the channel observed when R increases. This result may suggest that considering heterogeneous suspensions made of particles with different density ratio, we will find denser particle in the middle of the channel. When the density ratio crosses a threshold value ($\sim$100), we found a regime where the particles tend to be uncoupled with the fluid motions. In this "ballistic" regime the particle-particle interactions (collisions) are much stronger than the fluid-particle interactions and a further increase of the value of the density ratio slightly affects the general flow properties.

When the results were analyzed, various non-dimensional parameters were evaluated in order to find the best formula describing the transition

between the hydrodynamic and the ballistic regimes. The particle Stokes number $St \sim 100$ well discerns the conditions when the particle dynamics become uncoupled with the flow. However, since it does not include any relation with the volume fraction, it is not able to describe the different behaviors of the suspensions when ϕ is small but R is still large. Meanwhile, the Bagnold number does not perform well to describe the different flow behaviors when ϕ is kept constant and R is changed.

4.5 Future Developments

For a full comprehension of the present results further investigations are needed. Starting from the actual datas, it would be interesting to run longer the simulations with high density ratio, in order to analyze properly the local stresses along the wall-normal direction and to compare these results with those recently published by Picano et al. 2015 . Moreover, for a complete understanding of the physics driving the process additional simulations would be needed. For example, from the analysis of other cases with different values of ϕ and different density ratios it will be possible to fully characterize the transition from the hydrodynamic to the ballistic regimes. Meanwhile, a deeper analytical analysis would be requested in order to find a parameter well describing the whole transition process. Both the particle Stokes number and the Bagnold number failed in the interpretation of the results, but with the present datas it is not possible to conclude neither that they are completely unable to describe the transition when R increases, nor if a modification of their expressions would lead to a better match with the present results.

Appendix A

The Bagnold number

The Bagnold number was defined in Eq. (2.30):

$$Ba = \frac{\text{inertia stress}}{\text{viscous stress}} = \frac{\lambda^{1/2}\rho_p d_p^2 du/dy}{\mu_f} \tag{A.1}$$

The simplified expression found in Eq. (2.33) is deduced as follows:

$$\begin{aligned} Ba &= \frac{\lambda^{1/2}\rho_p d_p^2 du/dy}{\mu_f} \\ &= \lambda^{1/2}\frac{\rho_p}{\rho_f}\frac{\rho_f}{\nu_f}h^2\frac{du}{dy}\frac{d_p^2}{h^2} \\ &= \lambda^{1/2}\left(\frac{d_p}{h}\right)^2\frac{\frac{du}{dy}h^2}{\nu_f}R \\ &= 4\lambda^{1/2}\left(\frac{d_p}{h}\right)^2 Re_b R \end{aligned} \tag{A.2}$$

where Re_b is the bulk Reynolds number (1.28). In the previous derivation the following approximation was used:

$$\frac{du}{dy}h^2 \simeq 4u_b h \tag{A.3}$$

where the coefficient 4 is an approximation of the maximal value of the derivative of $\frac{du}{dy}$ at the wall.

Appendix B

The Stokes number

The Stokes number was defined in Eq. (2.29):

$$St_p = \frac{\text{particle characteristic time}}{\text{fluid characteristic time}} = \left(\frac{d_p^2 \rho_p}{18\nu_f}\right) / \left(\frac{h}{u_b}\right) \tag{B.1}$$

The simplified expression found in Eq. (2.32) is deduced as follows:

$$\begin{aligned} St_p &= \left(\frac{d_p^2 \rho_p}{18\nu_f}\right) / \left(\frac{h}{u_b}\right) \\ &= \frac{d_p^2}{18\nu_f} \frac{\rho_p}{\rho_f} \frac{u_b}{h} \\ &= \left(\frac{d_p}{h}\right)^2 \frac{1}{18} \frac{u_b h}{\nu_f} R \\ &= \left(\frac{d_p}{h}\right)^2 \frac{1}{18} Re_b R \end{aligned} \tag{B.2}$$

where Re_b is the bulk Reynolds number (1.28).

Appendix C

Total stress

The present appendix has been adapted from Picano et. al 2015 with the permission of the authors. In this work we used the framework developed by Prosperetti and co-workers to examine the stresses in the suspension (see Marchioro et al., 1999). Two different densities for the fluid (ρ_f) and for the particles (ρ_p) were assumed. Following Zang and Prosperetti (see Zang and Prosperetti, 2010), the phase indicators $\xi = 0$ for the fluid phase and 1 for the solid one were defined. The force balance for the volume $\mathcal{V}$ delimited by the surface $\mathcal{S}(\mathcal{V})$ reduces to:

$$\rho_p \int_{\mathcal{V}} \xi \mathbf{a}_p + \rho_f \int_{\mathcal{V}} (1-\xi)\mathbf{a}_f \, dV = \oint_{\mathcal{S}(\mathcal{V})} [\xi \boldsymbol{\sigma}_p + (1-\xi)\boldsymbol{\sigma}_f] \cdot \mathbf{n} \, dS \tag{C.1}$$

with $\mathbf{n}$ the outer unity vector normal to the surface $\mathcal{S}(\mathcal{V})$, the subscripts 'f' and 'p' denoting the fluid and the particle phases, $\mathbf{a}_i$ and $\boldsymbol{\sigma}_i$ the acceleration and the general stress in the phase i. Applying the phase ensemble average to Eq. (C.1), hereafter denoted as '$\langle\rangle$', it easy to obtain:

$$\rho_p \int_{\mathcal{V}} \langle \xi \mathbf{a}_p \rangle \, dV + \rho_f \int_{\mathcal{V}} \langle (1-\xi)\mathbf{a}_f \rangle \, dV = \\ = \int_{\mathcal{V}} \nabla \cdot [\langle \xi \boldsymbol{\sigma}_p \rangle + \langle (1-\xi)\boldsymbol{\sigma}_f \rangle] \, dV \tag{C.2}$$

where the divergence theorem was used to the differentiable integrand on the right hand side. Since the last equation holds for any mesoscale volume $\mathcal{V}$, it is possible to use the corresponding differential form of the equation:

$$\rho_p \langle \xi \mathbf{a}_p \rangle + \rho_f \langle (1-\xi)\mathbf{a}_f \rangle = \nabla \cdot [\langle \xi \boldsymbol{\sigma}_p \rangle + \langle (1-\xi)\boldsymbol{\sigma}_f \rangle] \tag{C.3}$$

Considering the definition of the volume fraction $\phi = \langle \xi \rangle$, the expression above can be further simplified:

$$\rho_p \phi \langle \mathbf{a}_p \rangle + \rho_f (1-\phi) \langle \mathbf{a}_f \rangle = \nabla \cdot (\phi \langle \boldsymbol{\sigma}_p \rangle + (1-\phi) \langle \boldsymbol{\sigma}_f \rangle) \tag{C.4}$$

Assuming the constitutive law of a Newtonian fluid $\boldsymbol{\sigma}_f = -p\mathbf{I} + 2\mu\mathbf{E}$ with p the pressure and $\mathbf{E}$ the symmetric part of the fluid velocity gradient tensor and considering that both the fluid and the particle velocity fields are divergence-free, Eq. (C.4) can be re-written as:

$$\frac{\rho_p}{\rho_f}\phi\left[\frac{\langle\mathbf{u}_p\rangle}{\partial t} + \langle\mathbf{u}_p\cdot\nabla\mathbf{u}_p\rangle\right] + (1-\phi)\left[\frac{\langle\mathbf{u}_f\rangle}{\partial t} + \langle\mathbf{u}_f\cdot\nabla\mathbf{u}_f\rangle\right] = \\ = \nabla\cdot\left(\phi\langle\frac{\boldsymbol{\sigma}_p}{\rho}\rangle\right) - (1-\phi)\frac{\nabla\langle p\rangle}{\rho_f} + \nu(1-\phi)\nabla^2\langle\mathbf{u}_f\rangle \tag{C.5}$$

The statistically stationary mean fluid and particle velocities are denoted as $\mathbf{U}_{f/p} = \langle\mathbf{u}_{f/p}\rangle$ and the fluctuations around these mean values are indicated as $\mathbf{u'}_{f/p} = \mathbf{U}_{f/p} - \langle\mathbf{u}_{f/p}\rangle$, so that the average momentum equation becomes:

$$\frac{\rho_p}{\rho_f}\phi\left[\mathbf{U}_p\cdot\nabla\mathbf{U}_p + \phi\nabla\cdot\langle\mathbf{u'}_p\mathbf{u'}_p\rangle\right] + (1-\phi)\left[\mathbf{U}_f\cdot\nabla\mathbf{U}_f + \langle\mathbf{u'}_f\mathbf{u'}_f\rangle\right] = \\ = \nabla\cdot\left(\phi\frac{\langle\boldsymbol{\sigma}_p\rangle}{\rho_f}\right) - (1-\phi)\frac{\nabla P}{\rho_f} + \nu(1-\phi)\nabla^2\langle\mathbf{u}_f\rangle, \tag{C.6}$$

with P the mean pressure.

Exploiting the symmetries of a fully developed parallel channel flow, characterized by two homogeneous directions (the streamwise, x and spanwise, z), it is possible to project Eq. (C.6) in the wall-normal direction y:

$$\frac{d}{dy}\left[(1-\phi)\langle v_f'^2\rangle + R\phi\langle v_p'^2\rangle + (1-\phi)\frac{P}{\rho_f} - \frac{\phi}{\rho_f}\langle\sigma_{p\,yy}\rangle\right] = 0. \tag{C.7}$$

Integrating Eq. (C.7) in the y direction and denoting by $P_w(x)$ the wall pressure, it is easy to obtain:

$$(1-\phi)\langle v_f'^2\rangle + R\phi\langle v_p'^2\rangle + \frac{P_T}{\rho_f} = \frac{P_w}{\rho_f}, \tag{C.8}$$

where $P_T = (1-\phi)(P/\rho_f) - \phi\langle\sigma_{P\,yy}\rangle/\rho_f$ is the mean total pressure. It should be noted that P_T coincides with P_w at the wall and that:

$$\frac{\partial P_T}{\partial x} = \frac{\partial P_w}{\partial x}. \tag{C.9}$$

Eq. (C.6) projected in the streamwise direction x reduces to:

$$\frac{d}{dy}\left[(1-\phi)\langle u_f'v_f'\rangle + R\phi\langle u_p'v_p'\rangle - \nu(1-\phi)\frac{dU_f}{dy} - \frac{\phi}{\rho_f}\langle\sigma_{p\,xy}\rangle\right] = -\frac{d}{dx}(\frac{P_w}{\rho_f}), \tag{C.10}$$

where the terms $(\partial/\partial x)\big[(\phi/\rho_f)(\langle\sigma_{p\,xx}-\sigma_{p\,yy}\rangle)\big]$ are neglected because of the streamwise homogeneity.

Integrating Eq. (C.10) in the wall normal direction and the denoting the Reynolds shear stress of the combined phase $\langle u'_C v'_C\rangle = (1-\phi)\langle u'_f v'_f\rangle + R\phi\langle u'_p v'_p\rangle$, the equation for the total stress $\tau(y)$ is obtained:

$$\tau(y) = -\langle u'_C v'_C\rangle + \nu(1-\phi)\frac{dU_f}{dy} + \frac{\phi}{\rho}\langle\sigma_{p\,xy}\rangle = \nu\frac{dU_f}{dy}\big|_w(1-\frac{y}{h}), \qquad \text{(C.11)}$$

where the boundary condition at the wall is $\tau_w = \tau(0) = \nu(dU_f/dy)|_{y=0}$. Eq. (C.11) shows that the total stress of a turbulent suspension in a channel geometry is given by three contributions: the viscous part, $\tau_V = \nu(1-\phi)(dU_f/dy)$, the turbulent part $\tau_T = -\langle u'_C v'_C\rangle = -(1-\phi)\langle u'_f v'_f\rangle - R\phi\langle u'_p v'_p\rangle$ and the particle-induced stress, $\tau_P = \phi\langle\sigma_{p\,xy}\rangle/\rho$. It should be noted that the turbulent stress accounts for the coherent streamwise and wall-normal motion of both fluid and solid phases. The particle induced stress is originated by the total stress exerted by the solid phase, see Eq. (C.1), and takes into account hydrodynamic interactions and collisions.

In the absence of particles, i.e. $\phi \to 0$, Eq. (C.11) reduces to the classic momentum balance for single-phase turbulence.

Acknowledgments

Grazie a Francesco e Luca per l'opportunità che mi avete dato. I vostri aiuti e i vostri consigli sono un dono prezioso di cui farò tesoro e per il quale vi sarò per sempre grato. Grazie anche a Walter, perché con me ha avuto davvero tanta, tanta pazienza.

Grazie a mia mamma e a mio papà, con cui litigo spesso, ma a cui in fondo voglio davvero bene. Mi avete sempre spronato e motivato a dare il massimo e senza questo incentivo, probabilmente, non sarei riuscito a fare tutto quello che ho fatto.

Grazie Anna, perché sei la sorella migliore di tutte.

Grazie al fantastico gruppo di Aerospaziali che l'Università mi ha fatto incontrare, ed in particolare Ilario, Pierpaolo, Fabio e Daniele. Perché sebbene lo studio ed il lavoro ci abbiano spinto agli antipodi del mondo, vi sento sempre vicini, come se fossimo ancora tutti insieme.

Grazie a tutti i pazzi che ho incontrato a Padova, ed in particolare Emanuele, Alberto, Matteo, Leni, Martina e Valeria. E' difficile trovare un aggettivo per descrivere come avete reso il mio ultimo anno a Padova. A voler proprio sceglierne uno, direi "esplosivo".

Grazie agli amici storici di Verona, Tommaso, Alessandro, Cecilia, Luna, Pietro, Giacomo, Francesca e Veronica. Perché sebbene le nostre vite stiano prendendo strade diverse, la vostra presenza rimane un punto di riferimento da cui non potrò mai prescindere.

Thank God, ce l'ho fatta!

Bibliography

[1] Frisch U. 1995. *Turbulence: the legacy of A.N. Kolmogorov.* Cambridge University Press.

[2] Kundu P.K., Cohen I.M. 2004. *Fluid Mechanics (3rd. edition).* Elsevier.

[3] Pope S.B.. 2000. *Turbulent Flows.* Cambridge University Press.

[4] Guazzelli E., Morris J.F.. 2011. *A Physical Introduction to Suspension Dynamics.* Cambridge University Press.

[5] Stokes G.G. 1851 *On the effect of the inertial friction of fluids on the motion of pendulums.* Trans. Cambridge Phil. Soc.

[6] Bagnold R. 1954. Proc. R. Soc. A **225**, 49.

[7] Batchelor G.K., Green J.T. 1972. *The hydrodynamic interactions of two small freely-moving spheres in a linear flow field.* J. Fluid Mech., **56**, 375-400.

[8] Batchelor G.K., Green J.T. 1972. *The determination of the bulk stress in a suspension of spherical particles to order c^2.* J. Fluid Mech., **56**, 401-427.

[9] Breugem W.P. 2012. *A second-order accurate immersed boundary method for fully resolved simulations of particle-laden flows.* J. Comput. Phys., **231**, 4469-4498.

[10] Eaton J.K. 2009. *Two-way coupled turbulence simulations of gas-particle flows using point-particle tracking.* nternational Journal of Multiphase Flow, **35**, 792?800.

[11] Kempe T., Schwarz S., Frohlich J. 2009. *Modelling of spheroidal particles in viscous flows.* Proceedings of the Academy Colloquium Immersed Boundary Methods: Current Status and Future Research Directions (KNAW, Amsterdam, The Netherlands, 15-17 June 2009).

[12] Koh C.J., Hookmam P., Leal L.G. 1994. *An experimental investigation of concentrated suspensions flows in a rectangular channel.* J. Fluid Mech., **266**, 1-32.

[13] Kolmogorov A.N. 1972. *Dissipation of energy in locally isotropic turbulence.* Dokl. Akad. Nauk SSSR 32, 19-21.

[14] Kolmogorov A.N. 1972. *The equations of turbulent motion in an incompressible fluid.* Izoestia Acad. Sci., USSR; Phys. 6, 56-58.

[15] Kulick J.D., Fessler J.R., Eaton J.K., 1994. *Particle response and turbulence modification in fully developed channel flow.* J. Fluid Mech., **277**, 109-134.

[16] Lashgari I., Picano F., Brandt L. 2014. *Laminar, Turbulent, and Inertial Shear-Thickening Regimes in Channel Flow of Neutrally Buoyant Particle Suspensions.* Physical review letters, **113**, 254502.

[17] Leighton D.T., Acrivos A. 1987. *Measurement of shear-induced self-diffusion in concentrated suspensions of spheres.* J. Fluid Mech., **177**, 109-131.

[18] Leighton D.T., Acrivos A. 1987. *The shear-induced migration of particles in concentrated suspensions.* J. Fluid Mech., **181**, 415-439.

[19] Marchioro M., Tankslay M., Prosperetti A. 1999. *Mixture pressure and stress in disperse two-phase flow.* Intl. J. Multiphase Flow, **25**, 1395-1429.

[20] Matas J., Morris J., Guazzelli E. 2003. *Transition to Turbulence in Particulate Pipe Flow.* Phys. Rev. Lett., **90**, 014501.

[21] Nott P.R., Brady J.F. 1994. *Pressure-driven flows of suspensions: simulation and theory.* J. Fluid Mech., **275**, 157-199.

[22] Oseen C.W. 1910. *Über die Stokessche Formel und über eine Verwandte Aufgabe in der Hydrodynamik.* Ark. Mat. Astron. Fys., **6**, No. 29.

[23] Oseen C.W. 1913. *Über den Goltigkeitsbereich der Stokessche Widerstandsformel.* Ark. Mat. Astron. Fys., **9**, No. 16.

[24] Paris A.D., Eaton J.K. 2001. *Turbulence Attenuation in a Particle-Laden Channel Flow,.* Report TSD-137, Dept. of Mechanical Engineering, Stanford University.

[25] Peskin C.S. 1972. *Flow patterns around heart valves: a numerical method.* J. Fluid Mech., **275**, 157-199.

[26] Picano F., Breugem W.P., Brandt L. 2015. *Turbulent channel flow of dense suspensions of neutrally buoyant spheres.* J. Fluid Mech., **764**, 463-487.

[27] Produman I., Pearson J.R. 1957. *Expansion at small Reynolds number for the flow past a sphere and a circular cylinder.* J. Comput. Phys., **10**, 252-271.

[28] Reynolds O. 1883. Phil. Trans. R. Soc. A **174**, 935.

[29] Rocco G. 2009. *Direct Numerical Simulations of turbulent lean premixed H2-flames with detailed chemistry.* Second Degree Thesis, Università degli studi di Roma "La Sapienza".

[30] Segré G., Silberberg A. 1962. *Behavior of macroscopic rigid spheres in Pouseuille flow. Part 2. Experimental results and interpretation.* J. Fluid Mech., **14**, 136-157.

[31] Semlitsch B. 2014. *Large eddy simulation of turbulent compressible jets.* Doctoral Thesis in Engineering Mechanics, KTH Royal Institute of Technology.

[32] Taylor G.I. 1922. *Diffusion by Continuous Movements.* Proceedings of the London Mathematical Society s220, 1.

[33] Uhlmann M. 2005. *An immersed boundary method with direct forcing for simulation of particulate flows.* J. Comput. Phys., **209**, 448-476.

[34] Yu Z., Wu T., Shao X., Lin J. 2013. *Numerical studies of the effects of large neutrally buoyant particles on the flow instability and transition to turbulence in pipe flow.* Phys. Fluids., **25**, 043305.

[35] Zang Q., Prosperetti A. 2010. *Physics-based analysis of the hydrodynamic stress in a fluid-particle system.* Phys. Fluids., **22**, 033306.